Activation of the mitochondrial unfolded protein response regulates the dynamic formation of stress granules

Marta Lopez-Nieto Jordana[1,2], Zhaozhi Sun[3], Rahme Safakli[4], Alessia Ruggieri[3], Ioannis Smyrnias[4,*] and Nicolas Locker[1,2,*].

[1] Faculty of Health and Medical Sciences, School of Biosciences and Medicine, University of Surrey, Guildford, United Kingdom.

[2] The Pirbright Institute, Pirbright, United Kingdom.

[3] Heidelberg University, Medical Faculty, Centre for Integrative Infectious Disease Research (CIID), Department of Infectious Diseases, Molecular Virology, Heidelberg, Germany.

[4] Faculty of Health and Medical Sciences, School of Veterinary Medicine, University of Surrey, Guildford, United Kingdom.

* Corresponding authors email: nicolas.locker@pirbright.ac.uk, i.smyrnias@surrey.ac.uk

Running title: the UPRmt regulates SG formation

Keywords: UPRmt, stress granules, integrated stress response, mitochondrial stress response, GADD34

Summary statement

We describe a novel crosstalk between the mitochondrial unfolded protein response and the integrated stress response involving stress granules that protects cells from further stress.

Abstract

To rapidly adapt to harmful changes to their environment, cells activate the integrated stress response (ISR). This results in an adaptive transcriptional and translational rewiring, and the formation of biomolecular condensates named stress granules (SGs), to resolve stress. In addition to this first line of defence, the mitochondrial unfolded protein response (UPRmt) activates a specific transcriptional programme to maintain mitochondrial homeostasis. We present evidence that SGs and UPRmt pathways are intertwined and communicate with each other. UPRmt induction results in eIF2α phosphorylation and the initial and transient formation of SGs, which subsequently disassemble. We show that the induction of GADD34 during late UPRmt protects cells from prolonged stress by impairing further assembly of SGs. Furthermore, mitochondrial respiration is enhanced during UPRmt activation when SGs are absent, suggesting that UPRmt-induced SGs have an adverse effect on mitochondrial homeostasis. These findings point to a novel crosstalk between SGs and the UPRmt that may contribute to restoring mitochondrial functions under stressful conditions.

Introduction

Controlling the localisation and function of macromolecules is fundamental for many cellular functions and typically achieved by surrounding them with lipid membranes in organelles such as the nucleus, lysosomes, or mitochondria. In recent years, biomolecular condensates that lack membranes have become increasingly recognised as an alternative way to organise cellular components during stress. The dynamic formation of these condensates is supported by networks of protein-protein, protein-RNA and RNA-RNA interactions, generating high local concentration of RNA and protein components (Tauber et al., 2020). With such remarkable molecular plasticity, biomolecular condensates provide an ideal platform for the regulation of key processes, including mRNA metabolism or intracellular signalling, and are utilised by cells to rapidly adjust and rewire regulatory networks in response to various physiological and pathological triggers (Yoo et al., 2019).

Stress granules (SGs) are among the most characterised cytoplasmic biomolecular condensates and assemble in response to many stresses, including oxidative stress, heat shock, viral infection, proteasomal inhibition, endoplasmic reticulum (ER) stress and UV irradiation (Corbet and Parker, 2019; Hofmann et al., 2020). Capturing mRNAs and proteins, SGs are central to the reorganisation of cellular contents during stress. Stress sensing results in the activation of the integrated stress response (ISR) and a global inhibition of protein synthesis usually driven by phosphorylation of the eukaryotic translation initiation factor 2α (eIF2α), which results in the dissociation of mRNAs from polysomes and their accumulation in cytoplasmic RNP complexes (Hofmann et al., 2020). These RNPs are then recognised by aggregation prone RNA-binding proteins (RBPs), such as Ras-GTPase activating SH3 domain binding protein 1 (G3BP1) and T cell internal antigen-1 (TIA-1), which lead to further recruitment of multiple proteins containing low sequence complexity domains or intrinsically disordered regions. These mediate clustering and fusion events driven by multivalent interactions between their protein and RNA components, at the core of which G3BP1 acts as a key node that promotes RNA-protein, protein-protein and RNA-RNA interactions, ultimately resulting in liquid-liquid phase separation (LLPS) and SG formation (Corbet and Parker, 2019; Wang et al., 2018). SGs are highly dynamic, rapidly assembling to sequester the cytoplasmic stalled mRNAs and dissolving upon stress resolution to release stored mRNAs for future translation (Matheny et al., 2019; Namkoong et al., 2018). The dynamic nature of SGs is also reflected in their proposed stress-selective compositional, structural and functional heterogeneity, with different stresses proposed to induce at least 3 distinct types of SGs (Aulas et al., 2017; Hofmann et al., 2020). Type I and II SGs assemble via eIF2α-dependent and independent pathways, respectively, while type III SGs lack eIFs and are associated with cellular death (Reineke and Neilson, 2019). This suggests that compositionally heterogeneous SGs support specialized functions promoting survival or pro-death outcomes. By concentrating specific protein components and altering their cytoplasmic concentration, SGs have been proposed to alter the course of biochemical reactions and signalling cascades (Hofmann et al., 2020). Furthermore, recent evidence hints that metabolic enzymes stored in SGs produce metabolites that can affect their stability (Begovich et al., 2020; Rollins et al., 2017; Saad et al., 2017). Importantly, dysregulation of pathways impacting SG clearance or LLPS is increasingly associated with neuropathology, in particular amyotrophic lateral

sclerosis and related diseases (Wolozin and Ivanov, 2019). Moreover, SGs can be exploited by cancer cells to adapt to the tumour microenvironment, with resident SG proteins aberrantly expressed in tumours (Anderson et al., 2015). Finally, SGs are also proposed to be a crossroad between intracellular signalling and antiviral responses by controlling the location and function of key sensors and effectors of innate immunity (Eiermann et al., 2020).

In addition to this first line of defence, cells have evolved tailored quality control processes to protect the functions of key organelles in times of stress. Mitochondria act as the cell's powerhouse, generating energy through oxidative phosphorylation but are also critical for essential function as such as calcium homeostasis, nucleotide metabolism and innate immunity regulation (Banoth and Cassel, 2018; Giorgi et al., 2018; Spinelli and Haigis, 2018). Key to maintaining or adapting mitochondrial functions, the mitochondrial unfolded protein response (UPRmt) is an evolutionarily conserved mitochondria-to-nucleus signalling cascade, initially described as a transcriptional response to the accumulation of misfolded mitochondrial proteins (Martinus et al., 1996; Zhao et al., 2002). Studies have shown that activation of the UPRmt is primarily regulated by the Activating Transcription Factor 5 (ATF5) (Fiorese et al., 2016; Smyrnias et al., 2019; Wang et al., 2019), and engaged upon a wide range of mitochondrial insults, including abnormal level of mitochondrial reactive oxygen species (ROS) (Wang et al., 2022b), dissipation of mitochondrial membrane potential (Rolland et al., 2019), and reduced mitochondrial protein import efficiency (Nargund et al., 2012). Activated UPRmt serves to restore mitochondrial protein homeostasis and promote cell survival in various biological processes, such as innate immune signalling (Pellegrino et al., 2014) and ageing (Houtkooper et al., 2013), as well as adaptation to pathophysiological conditions, such as neurodegenerative disorders (Sorrentino et al., 2017) and cardiovascular diseases (Smyrnias et al., 2019; Wang et al., 2019). Notably, growing evidence implicates the components of the ISR as central elements of the UPRmt (Anderson and Haynes, 2020; Fu et al., 2023; Quirós et al., 2017).

The ISR is an adaptive gene expression regulation programme activated in response to a range of pathophysiological conditions, including hypoxia, amino acid deprivation, and viral infection (Brostrom et al., 1996; Dever et al., 1992; Harding et al., 2003; Ron, 2002; Wek et al., 2006). ISR signalling is initiated by the phosphorylation of eIF2α by four different kinases, which results in global translational shut down to dampen cellular workload and accumulation of SGs, while specific transcripts involved in stress adaptation remain preferentially translated. A key aspect of ISR regulation involves the fine-tuning of eIF2α phosphorylation by the growth arrest and DNA-damage inducible protein (GADD34). This stress-induced regulatory subunit of protein phosphatase 1 (PP1) mediates eIF2α dephosphorylation, acting as a negative feedback loop to prevent prolonged ISR activation to ensure stress resolution and resuming of protein synthesis (Harding et al., 2000; Lee et al., 2009; Novoa et al., 2001). Studying the components of the ISR signalling has provided evidence that the ISR acts as an essential precursor to the UPRmt during mitochondrial stress. Specifically, each of the eIF2α kinases has been implicated in response to stress associated with mitochondrial dysfunctions (Baker et al., 2012; D'Souza and Minczuk, 2018; Guo et al., 2020; Samluk et al., 2019; Zhang et al., 2018). In addition, ATF5, together with ATF4 and C/EBP homologous protein (CHOP), are main regulators of the

ISR that have emerged as essential mediators of a response to mitochondrial dysfunction similar to the UPRmt in *C. elegans* (Fiorese et al., 2016; Jiang et al., 2020; Kaspar et al., 2021; Quirós et al., 2017; Zhao et al., 2002). Moreover, UPRmt activation following mitochondrial dysfunction has been linked to reduced protein synthesis within the mitochondria (Münch and Harper, 2016), and with studies demonstrating that SGs impact metabolic processes, act as signalling hubs, and dock to mitochondria, we propose that SGs may be implicated in the interface between UPRmt and ISR signalling during mitochondrial stress.

Herein, we established a novel crosstalk between the UPRmt and SGs. Induction of UPRmt during mitochondrial stress first results in an initial wave of SGs, which then disassemble potentially due to an upregulation of SG disassembly chaperones. Next, the negative feedback loop mediated by GADD34 protects cells against further stress insults and the assembly of eIF2α-dependent SGs. Finally, we demonstrated that the core SG scaffold proteins G3BP1 and G3BP2 (G3BP1/2) negatively affect mitochondrial respiration. Therefore, we propose a model in which the dynamic assembly of SGs is an important component of the UPRmt to maintain mitochondrial homeostasis, which itself can fine-tune further adaptation to stress by activating GADD34. This provides further understanding of the cellular adaptation to adverse conditions and the crosstalk between generalised and specialised stress responses.

Results

UPRmt activation following GTPP-mediated mitochondrial stress leads to induction of ISR signalling and is associated with transient SG assembly

With previous studies suggesting an interplay between the UPRmt and the ISR, and given the central role of SGs in the cellular stress response, we investigated the impact of mitochondrial stressors on the SG pathway in more details. First, we tested the induction of UPRmt signalling in U2OS cells following mitochondrial stress using the mitochondrial HSP90 inhibitor gamitrinib-triphenylphosphonium (GTPP), which results in protein misfolding in the mitochondria and induction of mitochondrial chaperones and proteases (Kang et al., 2009). The levels of typical transcripts induced upon UPRmt and ISR activation were measured using RT-qPCR (Fig 1A). We observed a clear induction of CHOP and ATF4 after GTPP treatment, which are related to ISR activation, as well as HSPD1 and LONP1, indicating induction of the UPRmt. ATF5 acts as a key mediator of the mammalian UPRmt signalling, translocating to the nucleus upon stress to activate a specific transcriptional cascade (Fiorese et al., 2016). Consistently, siRNA-mediated silencing of ATF5 expression significantly reduced the transcription of all GTPP-induced UPRmt markers, but not ISR markers, further supporting the role of ATF5 as UPRmt inducer in our model (Fig 1A).

Next, we tested the impact of UPRmt activation on SG assembly by treating U2OS cells with GTPP for up to 8 hours. Cells were fixed at the indicated time points and stained with anti-G3BP1 and anti-eIF3η antibodies to detect SG assembly (Fig 1B). Sodium arsenite was used as positive control for SG assembly as it induces eIF2α-dependent SGs by activating the eIF2α kinase HRI (Taniuchi et al., 2016). G3BP1 and eIF3η remained diffused in the cytoplasm in DMSO-treated cells and as expected, arsenite

treatment resulted in the assembly of SGs reflected by the accumulation of G3BP1/eIF3η into cytoplasmic foci. Interestingly, approximately 25% of cells were positive for SGs at 2 h post GTPP treatment (Fig 1C). The percentage of SG-positive cells decreased gradually until being undetectable at 8 h post treatment. Thus, mitochondrial stress following GTPP treatment in U2OS cells activates the UPRmt and induces an early and transient phase of SG assembly.

Phosphorylation of eIF2α is central event in the ISR signalling and a trigger of SG formation (Kedersha et al., 2002). Thus, we measured phosphorylation levels of eIF2α as well as protein and RNA expression levels of ISR markers during early UPRmt activation. Phosphorylation of eIF2α was detected within 30 minutes of GTPP treatment, which was followed by an increase of ATF4 protein levels and GADD34 in a later phase, at 3 h post treatment (Fig 2A). Similarly, CHOP mRNA levels were also highly upregulated from 2 h GTPP treatment, around 15-fold change, as well as GADD34 mRNA which reached 4-fold change upregulation at later time points (Fig 2B). These results suggest that UPRmt induction by GTPP signals through the early activation of canonical ISR. We therefore tested which of the four eIF2α kinases is activated during UPRmt induction. We first hypothesized that the double-stranded RNA (dsRNA)-activated protein kinase (PKR) might be activated upon GTPP treatment due to mitochondrial dsRNA leakage occurring as a consequence of mitochondrial stress and membrane damage (Kim et al., 2018). However, mitochondrial dsRNA was not detected after UPRmt induction (Fig 2C). Supporting this result, the expression of the interferon-stimulated genes such as CCXCL10, CCL5, MX1 and OAS1, reported to be induced upon PKR activation (Pindel and Sadler, 2011; Radetskyy et al., 2018), was not upregulated during early or late UPRmt (Fig 2D). Thus, PKR is unlikely to be the kinase responsible for eIF2α phosphorylation upon GTPP treatment. We next investigated the potential role of PKR-like ER kinase (PERK) and general control non-derepressible protein 2 (GCN2). PERK is activated in response to ER stress and has been shown to modulate mitochondrial homeostasis during stress (Almeida et al., 2022), while general control non-derepressible protein 2 (GCN2) is activated by amino acid depravation or UV light radiation (Deng et al., 2002). We used the pharmacological inhibitors GSK2606414 and A-92 to inhibit PERK and GCN2 activity in U2OS cells, respectively. We first confirmed that they reduced eIF2α phosphorylation upon DTT treatment or UV light exposure (Fig 2E). In response to GTTP, the GCN2 inhibitor A-92 did not reduce eIF2α phosphorylation, whereas the PERK inhibitor GSK2606414 decreased it by more than 2-fold, suggesting that PERK is the main eIF2α kinase responsive to GTTP. Overall, these results suggest that induction of the UPRmt is associated with an early SG assembly and ISR activation through PERK.

<u>Mitochondrial stress impairs the assembly of eIF2α-dependent SGs</u>

As GTPP-mediated mitochondrial stress and UPRmt activation resulted in SG assembly only during the early and not at the later stages of stress, we hypothesized that the UPRmt may limit the ability of cells to form SG during prolonged stress. To test this, cells were stimulated for 4, 6 or 8 h with GTPP and then challenged with or without arsenite for 30 min (Fig 3A). As expected, in absence of pre-treatment with GTTP, arsenite induced the assembly of SGs in almost all cells. Interestingly, only few GTTP-treated cells formed SGs after arsenite treatment at the indicated timepoints. Detailed analysis of U2OS cells revealed that pre-treatment with GTPP reduced arsenite-induced SG assembly compared to

arsenite-only stimulated cells from 90 to 14%, 95 to 28% and 91% to 35% after 4, 6 or 8 h treatments, respectively (Fig 3B). These data indicate that UPRmt induction by GTPP inhibits subsequent arsenite-induced SG formation. Given that eIF2α phosphorylation drives SG formation, we next assessed how UPRmt activation impacts on arsenite-induced eIF2α phosphorylation. Cells were treated as mentioned above and levels of basal and phosphorylated eIF2α measured by immunoblotting. Cells treated with arsenite displayed high levels of eIF2α phosphorylation, while GTPP treatment slightly increased eIF2α phosphorylation as shown previously (Fig 3C). Interestingly, when subjected to arsenite treatment, GTPP pre-treated cells showed lower levels of arsenite-induced eIF2α phosphorylation. Specifically, phosphorylated levels were reduced approximately 3 to 4-fold compared to arsenite-treated cells in all timepoints.

To confirm these results, UPRmt was induced with another mitochondrial stressor, paraquat, which produces high amounts of superoxide and interferes with the electron transport chain (Cocheme and Murphy, 2008). Treatment of cells with paraquat for 48 h increased by 2 to 3-fold the mRNA levels of ATF4, CHOP, GADD34 and DNAJA3 compared to non-treated cells, confirming ISR and UPRmt activation (Sup Fig 1). Next, we examined how paraquat stimulation impacts on SG assembly and whether pre-treatment with paraquat affects the ability of cells to form arsenite-induced SGs by immunofluorescence. Paraquat treatment did not induce SG formation, and G3BP1 or eIF3η remain diffused in the cytoplasm (Fig 3D). However, prior induction of UPRmt by paraquat pre-treatment decreased percentage of cells containing arsenite-induced SGs, from about 96% to 65% (Fig 3E). Similarly to GTPP-induced mitochondrial stress, paraquat treatment also resulted in a slight increase in eIF2α phosphorylated levels, supporting ISR induction and pre-treatment with paraquat also limited the levels of arsenite-induced eIF2α phosphorylation compared to non-treated cells (Fig 3F). Overall, activation of UPRmt using two different stressors resulted in the inhibition of arsenite-induced eIF2α phosphorylation and consequently prevents SG formation during prolonged stress.

SG assembly is a multistep process by which first “seeds”, invisible microscopically, coalesce upon stress, and then fuse into larger aggregates during a growth phase (Wheeler et al., 2016). We next examined whether the SG maturation process was also affected by paraquat. To address this, the average size and number of SGs per cell from paraquat pre-treated cells were compared to non-treated cells. The analysis revealed that arsenite-induced SGs are significantly smaller (in average 0.53 μm^2) in paraquat pre-treated cells compared to those formed in non-treated cells (in average 0.85 μm^2). In addition, more G3BP1-positive SGs per cell were detected in paraquat pre-treated cells compared to non-treated (in average 57 vs 32, respectively) (Fig 3G). These results indicate that paraquat impairs SG formation and limits their maturation into larger SGs. Altogether, these data strongly support that SG assembly is modulated by prior induction of the UPRmt.

Given that ATF5 is one of the central regulators in UPRmt activation, we explored its impact on SG assembly (Fiorese et al., 2016). To study this, cells were transfected with siRNA targeting ATF5 and SG formation was monitored by immunofluorescence during GTPP treatment for 4 h and with or without arsenite stimulation (Sup Fig 2A). ATF5 silencing did not affect SG assembly nor disassembly after 4 h of GTPP treatment, around 20% of cells were positive for SGs (Sup Fig 2B). Moreover, prior induction

of UPRmt assembly of arsenite-induced SGs was impaired when ATF5 was silenced, with no differences compared to control cells. These findings suggest that the UPRmt transcriptional reprogramming associated with ATF5 activation is not involved in the modulation of SG assembly nor disassembly, and that other UPRmt factors contribute to SG dynamics.

GADD34 is required for the inhibition of *de novo* eIF2α-dependent SG assembly by preventing eIF2α phosphorylation

We observed that UPRmt activation by either GTPP or paraquat results in the upregulation of GADD34 (Fig 2A, 2B and Sup Fig 1), the negative regulator of the ISR, which in complex with PP1 dephosphorylates eIF2α to resume translation. Therefore, we hypothesized that increased levels of GADD34 could limit eIF2α phosphorylation in response to a consecutive stress and consequently SG assembly. To test this hypothesis, we generated U2OS GADD34 KO cell clones using a CRISPR/Cas9 approach (Sup Fig 3). Control cell clones (Ctrl) were generated for comparison using a non-targeting crRNA. Ctrl and GADD34 KO cells were stimulated with GTPP for 4 h prior arsenite treatment and SG assembly detected by immunofluorescence (Fig 4A). As observed previously, prior induction of UPRmt by GTPP impaired the assembly of arsenite-induced SGs in Ctrl cells. In contrast, we observed no difference in the assembly of SGs in GADD34 KO cells irrespectively of GTTP pre-treatment. While only 17% of Ctrl cells pre-treated with GTPP were positive for arsenite-induced SG, 97% of GADD34 KO cells contained SGs in the same conditions (Fig 4B). Similar results were obtained with paraquat pre-treatment with 66% Ctrl cells and 98% GADD34 KO cells displaying SGs in response to arsenite treatment (Fig 4C, 4D).

These results were supported by reduced levels of phosphorylated eIF2α in GTTP and paraquat pre-treated Ctrl cells compared to GADD34 KO cells (Fig. 4E, 4F). In Ctrl cells, either GTPP or paraquat treatment followed by arsenite stimulation resulted in reduced eIF2α phosphorylation levels compared to stimulation with arsenite only. In contrast, in GADD34 KO cells, the induction of eIF2α phosphorylation was comparable between stimulation with arsenite and GTPP or paraquat treatments followed by arsenite stimulation. Therefore, GADD34 KO rescued the ability of cells to phosphorylate eIF2α following UPRmt induction. Overall, these results indicate that UPRmt activation results in increased levels of GADD34 expression, which prevent eIF2α phosphorylation and impair the ability of cells to assemble SGs in response to prolonged stress.

GTPP-mediated UPRmt activation differentially modulates the assembly of eIF2α-independent SGs

SG assembly can also be triggered following eIF2α-independent inhibition of translation, for example by blocking eIF4A or mTOR activity (Aulas et al., 2017). Thus, we examined whether UPRmt activation alters the assembly of eIF2α-independent SGs following treatment with the eIF4A inhibitor silvestrol (Bordeleau et al., 2008). To test this, U2OS cells were stimulated with GTPP for 6 h, then treated with or without silvestrol for 1 h and SG assembly was analysed by immunofluorescence (Fig 5A). As expected, silvestrol induced formation of SGs in nearly all cells. Interestingly, pre-treatment with GTPP resulted in a reduction of the percentage of cells displaying silvestrol-induced SGs, from 94% to 72% (Fig 5B). In contrast, pre-treatment with paraquat did not impair the assembly of silvestrol-induced SGs.

(Fig 5C, 5D). However, features of SGs appeared to be altered by paraquat treatment, as reported before for arsenite-induced SGs, with reduction in average size, from 0.97 μm^2 to 0.66 μm^2, and increased average number, from 18 to 39, when compared to non-treated cells (Fig 5E). These results indicate that UPRmt activation by GTPP impairs the ability of cells to assemble eIF2α-independent SGs, although not to the same extent as eIF2α-dependent SGs, and that paraquat affects their maturation and fusion process. Taken together, these data suggest that UPRmt activation impact on SG assembly and dynamics both in an ISR-dependent and -independent manner.

SGs are highly dynamic and disassemble upon stress removal. Recently, the chaperone Hsp90 was reported to initiate SG disassembly by interacting with and activating the dual specificity tyrosine-phosphorylation-regulated kinase 3 (DYRK3), leading to the phosphorylation of yet unknown targets. (Mediani et al., 2021). Given that GTPP-induced SGs disassemble after 4 h treatment (Fig 1C) and to further examine how UPRmt activation modulates assembly and dynamics of eIF2α-independent SGs, we measured the mRNA levels of DYRK3 and the stress-inducible and constitutively expressed Hsp90 forms, HSP90AA1 and HSP90AB1, respectively. Upon UPRmt induction by GTPP, the level of HSP90AA1 mRNA was significantly increased by approximately 4 to 6-fold in all time points compared to non-treated cells, while Hsp90AB1 and DYRK3 were slightly upregulated by 2 to 3-fold at 6 and 8 h GTPP treatment (Figure 5F). In contrast, the mRNA expression of these proteins remained unchanged upon UPRmt induction by paraquat (Figure 5G). These results are consistent with our previous results where silvestrol-induced SG assembly was altered by GTPP treatment but not by paraquat, indicating that UPRmt activation by GTPP results in enhancement of SG disassembly process which might be involved in the modulating the assembly of eIF2α-independent SGs, while paraquet did not. Altogether, these data suggest that UPRmt activation by GTPP results in an initial SG assembly which then rapidly disassemble potentially due to an enhancement in the SG disassembly process.

<u>Cells unable to assemble SGs during stress present with improved mitochondrial function during UPRmt activation</u>

To determine the functional consequences of reduced SG formation during mitochondrial stress, we compared mitochondrial respiration upon UPRmt activation in U2OS G3BP1/2 double knockout cells (G3BP1/2 dKO) lacking the ability to form SGs to control cells (Yang et al., 2020) (Sup Fig 4). Wild-type (WT) and G3BP1/2 dKO U2OS cells were treated with GTPP for 2 h, the time at which we previously detected the appearance of SGs, and measured mitochondrial oxygen consumption rate (OCR) using a Seahorse flux analyser (Fig 6A). As expected GTTP treatment impaired mitochondrial functions in WT cells resulting in decreased basal, maximal respiration, ATP-linked respiration and spare respiratory capacity compared to untreated cells (Fig 6B, 6C). In contrast, G3BP1/2 dKO cells that cannot form SGs presented with significantly improved mitochondrial respiration when compared to WT cells when challenged with GTTP (Fig 6C). Taken together, these results indicate that the assembly of UPRmt-induced SGs is associated with impaired mitochondrial functions during stress.

Discussion

The disruption of mitochondrial homeostasis is associated with several pathologies, such as neurodegeneration, cancer, aging, and cardiovascular diseases (Chen et al., 2023; Norat et al., 2020; Quirós et al., 2016; Suomalainen and Battersby, 2018). The UPRmt is an evolutionarily conserved homeostatic pathway engaged upon a wide range of mitochondrial insults, including mitochondrial protein misfolding (Zhao et al., 2002), reduced mitochondrial protein import efficiency (Nargund et al., 2012), dissipation of mitochondrial membrane potential (Donehower et al., 2019), and dysregulated levels of reactive oxygen species (ROS) (Wang et al., 2022b). UPRmt activation triggers a broad and protective transcriptional cascade, through enhancing mitochondrial folding capacity and triggering a mitochondrial recovery program, alleviating neurodegenerative and cardiovascular diseases symptomatology (Smyrnias et al., 2019; Sorrentino et al., 2017), promoting resistance to pathogen infection (Mahmud et al., 2020; Pellegrino et al., 2014), and prolonging lifespan (Munkácsy and Rea, 2014). Studies in mammals have shown that the ISR and UPRmt are intertwined; however, how SGs – which are downstream effectors of the ISR – modulate the outcome of the UPRmt and how their assembly is regulated upon mitochondrial stress is unknown. Evidence supporting a functional interplay between SGs and mitochondria include the impaired metabolism linked to altered SG dynamics in several neurodegenerative diseases, the regulation of SG stability by metabolites produced by resident SG enzymes such as Sam1 or pyruvate kinase, and the regulation of mitochondrial permeability and lipid fatty acid oxidation by starvation-induced SGs (Begovich et al., 2020; Cereghetti et al., 2021; Rollins et al., 2017; Saad et al., 2017; Wang et al., 2022a). SGs can physically contact different membrane-bound organelles, including lysosomes or the ER, and starvation-induced SGs contact with mitochondria in human cells (Amen and Kaganovich, 2021; Lee et al., 2020; Liao et al., 2019). Furthermore, numerous mitochondrial proteins have been associated with SGs (Amen and Kaganovich, 2021; Aoyama-Ishiwatari et al., 2021; Paget et al., 2023). Our study identifies SGs as novel signalling components associated with the mammalian UPRmt and SG dynamics as a key for maintaining mitochondrial function during mitochondrial stress. We show that UPRmt activation by GTPP or paraquat results in PERK-mediated activation of the ISR, accompanied with transient SG formation, in the case of GTTP. Moreover, UPRmt-induced upregulation of the GADD34 protects cells against persistent SG assembly and preventing SG formation improved mitochondrial functions upon UPRmt induction.

ATF5 has been proposed to drive the protective effect of UPRmt in different diseases models such as osteoarthritis (Zhou et al., 2022), heart failure (Smyrnias et al., 2019; Wang et al., 2019), and protect host during enteric infection (Chamseddine et al., 2022). In our experimental system, we show that ATF5 is essential for the upregulation of the UPRmt markers in cells subjected to mitochondrial stress but is not involved in SG dynamics. Recently, a study by Sutandy *et al.* proposed that the accumulation of mitochondrial protein precursors and ROS in the cytosol results in nuclear translocation of heat shock factor 1 (HSF1) and activation of UPRmt markers. ATF5 synergises with HSF1, affecting late activation of the UPRmt (Sutandy et al., 2023). Thus, we cannot exclude the possibility that other transcription factors such as HSF1 may contribute to SG dynamics during induction of the UPRmt.

The disassembly of SGs is crucial for cellular homeostasis since persistent SGs can promote the formation of aberrant aggregates, which are implicated in several neurodegenerative diseases (Baron et al., 2013; Repici et al., 2019; Vanderweyde et al., 2012). SGs induced by GTPP begin to disassemble post 3 h treatment and completely disappear by 8 h. We first hypothesized that the increased expression of GADD34 due to ISR activation might be responsible for SG disassembly in these mid/late phases. However, GADD34 KO cells cleared SGs with a comparable kinetic to control cells (Fig 5), indicating that a factor other than GADD34 is involved in SG disassembly after GTPP treatment. In fact, GTPP resulted in increased expression of the kinase DYRK3, and HSP90, a major chaperone promoting SG disassembly of SGs through binding and stabilising DYRK3 (Mediani et al., 2021; Wippich et al., 2013). Upregulation of SG disassembly chaperones was not detected with paraquat, consistent with this stressor not inducing SG formation. Interestingly, UPRmt induction by either GTTP or paraquat prevented *de novo* assembly of arsenite-induced SGs by impairing eIF2α phosphorylation. This effect was rescued in GADD34 KO cells, indicating that GADD34 upregulation is responsible for the inhibition of SG assembly following a second stressor. This result is in line with recent work demonstrating that sustained GADD34 levels upon ISR activation reduces cell responsiveness to a second stress pulse, promoting cell adaptation (Klein et al., 2022). Our data suggest that UPRmt employs GADD34 as a negative regulator of the ISR to fine-tune cellular stress responses and maintain mitochondrial function under these conditions.

Furthermore, UPRmt activation by GTPP also inhibited the formation of eIF2α-independent SGs, and, the size and number of both eIF2α-dependent and independent SGs were altered in cells treated with paraquat compared to non-treated. This suggests that paraquat-induced stress could alter SG biogenesis by limiting the growth of small SGs prior to their fusion into bigger aggregates. We speculate that the known paraquat effects on oxidative phosphorylation could affect SG biogenesis, whose fusion and growth steps are ATP-dependent (Jain et al., 2016). Further experiments are needed to fully understand how energy depletion affects SG biogenesis during mitochondrial stress.

Our results reveal that cells subjected to mitochondrial stress activate the UPRmt and engage mechanisms to disassemble either SGs induced by mitochondrial stress and/or prevent *de novo* assembly of SGs, suggesting that clearance of SGs is crucial to the maintenance of mitochondrial homeostasis. Consistently, we show that GTPP-induced SGs impaired mitochondrial respiration, whereas cells unable to form SGs exhibited improved mitochondrial function during stress. Questions remain as to the functional link between inhibition of SG assembly and mitochondrial homeostasis following UPRmt activation. Several studies support a protective role for SGs, through impairing pro-apoptotic JNK signalling (Arimoto et al., 2008; Kitajima et al., 2023), sequestration of caspases (Fujikawa et al., 2023) or suppressing production of ROS (Park and Shin, 2023; Takahashi et al., 2013) and they have been described as “shock absorbers” dampening excessive innate immune response to viral infection (Paget et al., 2023). In contrast, persistent SGs are implicated in pro-death functions during chronic stress conditions as well as neurodegenerative diseases or tumour chemotherapy (Reineke et al., 2018; Reineke and Neilson, 2019; Schwed-Gross et al., 2022). Future studies will aim to the function of SGs formed during mitochondrial stress.

Overall, our findings support a model in which UPRmt-induced SGs are formed as a consequence of the associated ISR activation. Subsequently, cells activate mechanisms to disassemble SGs, as their persistence may compromise mitochondrial recovery. This could be by either physically preventing efficient mitochondrial dynamics, recruiting mitochondrial or related proteins to SGs, preventing translation of essential mitochondrial proteins, or a combination of all of them. This underscores a novel functional interplay between the ISR and UPRmt and further work should aim at revealing the impact of SG signalling during UPRmt, how UPRmt-induced SGs, and the sequestration of specific resident proteins, impact on mitochondrial homeostasis. This will open further opportunities for alternative strategies for the treatment of human diseases with compromised mitochondrial function and associated with an impaired SG dynamics.

Material and methods

Cell culture and gene silencing

U2OS, U2OS G3BP1/2 double knock out (dKO), U2OS control (Ctrl) and GADD34 KO cell lines were grown in Dulbecco's modified Eagle's medium (DMEM) supplemented with 10% fetal bovine serum, 100 U/ml penicillin, 100 g/ml streptomycin and 1% L-glutamine in a humidified incubator at 37ºC and 5% CO_2 environment. U2OS G3BP1/2 dKO cells have been described previously (Burke et al., 2020).

Silencing of ATF5 was performed using Lipofectamine-RNAiMax transfection reagent (Thermo Fisher). U2OS cells were incubated with the transfection mix containing either siRNA negative control (Invitrogen, #4390843) or siRNA targeting ATF5 (Invitrogen, ID s22425) at a final concentration of 10 nM for 48 h. Next, cells were incubated with subsequent treatments and analysed as described below.

Generation of U2OS GADD34 KO cell clones

U2OS GADD34 KO cells were generated using a two-crRNA strategy to delete a portion of the *PPP1R15A* locus encoding GADD34. crRNAs cutting sequences in *PPP1R15A* exon 2 (IDT, Hs.Cas9.PPP1R15A.AC: AltR1 / AUC ACU GGG UUG GCA CCA CCG UUU UAG AGC UAU GCU / AltR2) and exon 3 (IDT, custom design: AltR1 / GAG GCG UGG CUG AGA CCA ACG UUU UAG AGC UAU GCU / AltR2) were purchased to Integrated DNA technologies (IDT). Individual crRNAs and tracrRNA (IDT) were resuspended in 1 x TE buffer (10 mM Tris, 0.1 mM EDTA, pH 7.5) to a final concentration of 200 µM and hybridized at equimolar amounts by heating to 95 °C for 5 min and slow stepwise cooling (1°C/sec) to room temperature. Pre-assembled crRNA/Cas9 ribonucleoprotein complexes (RNPs) were obtained by gently mixing 1.2 µl of hybridized RNAs with 17 µg of recombinant Alt-R Cas9 protein (IDT) and 2.1 µl of PBS, followed by 20 min incubation at room temperature.
U2OS cells (1 x 10^6) were washed with PBS, resuspended in 91 µl nucleofection solution from Cell Line Nucleofector Kit V (Lonza) and mixed with 2.5 µl of each pre-assembled RNPs and 4 µl electroporation enhancer (Integrated DNA technologies). Nucleofection was performed using an Amaxa 2b nucleofector (Lonza) and pre-set program X-01. Nucleofected cells were incubated for 48 h prior to clonal amplification and screening for homozygous clones using target-specific PCR (GoTaq Hot Start, Promega) on genomic DNA using the following primers: PPP1R15A_forward: 5'-ATCACACCGGGAGTGTTGTC-3', PPP1R15A_reverse: 5'-AGACGCTGCTCGCTACAAAT-3')

flanking sequences targeted by crRNAs. After genotyping, expression levels of GADD34 in 2 control and 5 GADD34 KO single cell clones in response to 2 µM thapsigargin (Biotrend) treatment for 3 h was assessed by Western blotting. After characterization and for further experiments, cell pools were generated by mixing the clones in equal proportions.

Chemical treatments

For UPRmt induction, GTPP (kindly provided by I. Smyrnias) was diluted in DMSO and used at concentration of 10 µM for up to 8 h. Paraquat (Sigma-Aldrich, #36541) was dissolved in H_2O and used at a concentration of 0.5 mM for 48 h. For SG assembly, sodium arsenite (Sigma Aldrich) was diluted in H_2O and used at a concentration of 0.5 mM for 30 min. Silvestrol (MedChemExpress) was resuspended in DMSO and used at a concentration of 2 µM for 1 h. Phosphorylation of eIF2α was induced by DTT (Promega, DMSO) at 5 mM for 2 h or by UV irradiation at 20 mJ/cm2 using Stratalinker 1800 (Stratagene) followed by 2 h incubation at 37 ºC. GCN2 activity was inhibited using 1 µM A-92 (Merck, dissolved in DMSO). PERK activity was inhibited using 0.1 µM GSK2606414 (Merck, dissolved in DMSO).

Transfection with double-stranded (ds) RNA

Synthesis and purification of 200-bp dsRNA was described previously (Klein et al., 2022). In brief, a 200-bp region from the ampicillin resistance gene was used as template for *in vitro* synthesis of plus and minus strand transcripts, hybridized and purified. 2 x 10^5 cells were seeded in a 6-well plate containing coverslips and transfected with 1 µg dsRNA mixed with Lipofectamine 2000 transfection reagent (Thermo Fisher Scientific) in a 1:3 ratio. Cells were fixed after 16 h with PBS-PFA 4% and further processed for immunofluorescence analysis.

Immunofluoresence microscopy

Cells were seeded on sterilized coverslips in a 24-well plate and treated as required. Media was removed and fixed with 4% paraformaldehyde (PFA) in PBS for 20 min at RT. Fixation solution was removed, coverslips were rinsed with PB and stored at 4 ºC or processed immediately. Cells were permeabilized with 0.1% Triton X-100 (Sigma) in PBS for 5 min at RT and blocked with 0.5% bovine serum albumin (Fisher) in PBS for 1h at RT. Cells were then incubated with primary antibody solution for 1h at RT, washed 3 times with PBS and incubated with secondary antibody solution containing 0.2 µg/ml DAPI for 1h at RT. Coverslips were then rinsed 3 times with PBS and mounted onto microscope slides with 5 µl Mowiol 4-88 (Sigma-Aldrich #81381). Cells were visualized and imaged with a Nikon Ti-Eclipse A1M Confocal Microscope using a 60X objective. Confocal images were analysed utilizing Image J. SG quantification was either performed manually counting at least 100 cells per condition or automatically using the Analyze Particles function, obtaining further information such as the average size of SG and number per cell. The primary antibodies used were rabbit anti-G3BP1 (1:600, Sigma) and goat anti-eIF3η (1:600, Santa Cruz), rabbit anti-TOMM20 (1:1000, abcam), mouse IgG2a anti-dsRNA (1:250, SCICOBS), mouse IgG1 anti-TOMM20 (1:100, Becton Dickinson). Secondary antibodies used were goat anti-rabbit Alexa 488, donkey anti-goat Alexa 555, goat anti-mouse-IgG2 Alexa 568 and goat anti-mouse-IgG1 Alexa 488 (1:500, Invitrogen).

Immunoblotting

Cells were seeded in 6-well plates to be around 80-90% confluent at the indicated times. Cells were treated as required, then media was removed, and cells were washed twice with cold PBS. Cells were lysed with protein lysis buffer (50 mM Tris-HCl, 250 mM NaCl, 5 mM EDTA, 1 mM Mg_2Cl, 1% NP40 and supplemented with protease inhibitor cocktail, Roche), incubated on ice for 20 minutes and spun at 10,000 g for 10 min at 4 ºC. Supernatant was collected and protein concentration was measured following BCA pierce kit (Fisher) and between 20-60 µg of protein were used depending on the experiment and quantity obtained. Lysed were mixed with 3x red Loading buffer supplemented with DTT (Cell Signalling) and boiled at 95 ºC for 5 min. Lysates were separated in 4-20% gradient gel with 1x SDS running buffer and proteins were transferred to a nitrocellulose membrane using the Pierce Power Station and 1-step Transfer Buffer (Thermo Scientific). Membranes were blocked in 5% BSA or 5% marvel in TBS-Tween (TBS-T) for 1 h at RT and then incubated with primary antibodies overnight at 4 ºC. Next day, membranes were washed 3 times with TBS-T and subsequently incubated with secondary antibodies (Dako, 1:5000) diluted in 5% marvel in TBS-T for 1 h at RT. After three washes with TBS-T, secondary antibodies were labelled with Clarity Western ECL Substrate (Bio-Rad), and membranes were imaged using the vilber-Lourmat Imaging system. Band intensity was quantified and analysed using Image Lab Software (Bio-rad). Primary antibodies used were rabbit anti-eIF2α (1:1000, Cell Signaling), rabbit anti-P-eIF2α (1:1000, Invitrogen), rabbit anti-ATF4 (1:1000, Cell Signaling), rabbit anti-GADD34 (1:1000, Proteintech), mouse anti-GAPDH (1:5000, Ambion), goat anti-eIF3η (1:2000, Santa Cruz) and anti-eIF3A (1:2000, Bethyl Laboratories).

Preparation of RNA samples and RT-qPCR

Cells were seeded in 6-well plates to be around 80-90% confluent at the indicated times. Cells were treated as needed, then were washed twice with cold PBS, and total RNA was extracted using a quick-RNA micro prep kit (Zymo Research) following the manufacturer's instructions. Purified RNA was quantified on Nanodrop, and 500 ng of RNA was subject to reverse transcription using Precision nanoScript2 Reverse Transcription kit from Primer Design. Next, real-time quantitative PCR (qPCR) was performed in duplicate with 25 ng of template, specific primers listed below used at a final concentration of 0.3 µM and Precision Plus Master Mix (Primer Design) following manufacturer's instructions, using the Quant Studio 7 Flex (Applied Biosystems). The comparative Ct method was used; Ct values from genes of interest were normalized to RpL9 Ct values unless otherwise specified. The 2-ΔΔCT method was used to calculate the fold change expression relative to non-treated (Livak and Schmittgen, 2001).

Mitochondrial respiration

Oxygen consumption rate of U2OS WT and G3BP1/2 dKO cells was measured on an extracellular flux analyzer (Agilent Seahorse) using the XF Cell Mito Stress Test Kit following manufacturer's protocol. Cells were seeded one day prior the experiment on Seahorse XFe24 culture plate to be 80% confluent. Cells were treated as required and 1 h prior running the plate, medium was removed, and cells were incubated with assay medium supplemented with 1 mM pyruvate, 2 mM glutamine and 10 mM glucose. Cells were then sequentially stimulated with oligomycin at 1 µM, FCCP at 2 µM and rotenone and

antimycin A at 1 µM and respiratory profile was obtained. Data was normalised by amount of protein for each well. Following assay, cells were lysed with protein lysis buffer (50 mM Tris-HCl, 250 mM NaCl, 5 mM EDTA, 1 mM Mg_2Cl, 1% NP40 and supplemented with protease inhibitor cocktail, Roche), incubated on ice for 20 minutes and spun at 10,000 g for 10 min at 4 ºC. Supernatant was collected and protein concentration was measured following BCA pierce kit (Fisher).

Statistical analyses

Statistical analyses were performed using Graphpad Prism software and three biological replicates were analysed in all experiments. Statistical tests performed are indicated in the figure legends (****, P < 0.0001; ***, P < 0.001; **, P < 0.01; *, P < 0.05; ns, not significant).

Primer list

GENE	FORWARD PRIMER (5'→3')	REVERSE PRIMER (5'→3')
ATF4	GCTAAGGCGGGCTCCTCCGA	ACCCAACAGGGCATCCAAGTCG
ATF5	TTTGCAGTGCGGGAAGAT	AAAATGAACACCCAGTCACCA
CHOP	GGAGCATCAGTCCCCCACTT	TGTGGGATTGAGGGTCACATC
DNAJA3	GAGGACGAGACAGATGTGGAG	TCCTGCGGAGCTATCCAT
DYRK3	TCCTTCTGAACCACCTCCAC	CCTTCATCTCACCTCCATCC
GADD34	CAGAAACCCCTACTCATGATCC	AAATGGACAGTGACCTTCTCG
HSPD1	GATGGAGAAGCTCTAAGTACACTCG	GCTGGTTCTTTCTATTGTCACCA
HSP90AA1	ATGGCAGCAAAGAAACAC	GTATCATCAGCAGTAGGGTCA
HSP90BB1	TGGCAGTCAAGCACTTTTCTGT	GCCCGACGAGGAATAAATAGC
LONP1	AACGTGTCGGGCTACGTG	CTCTCATCCAAGCCACACAG
RPL9	GGTGGGGTAACAGAAAGGAAC	CGTTGATGGGGAAGTGAGC
RPS18	CCAAGAGGGCGGGAGAAC	TATTTTCCATCCTTTACATCCTTCTG
CCL5	ACGTCAAGGAGTATTTCTACAC	GATGTATTCTTGAACCCACT
CXCL10	TGGCATTCAAGGAGTACCTC	TTGTAGCAATGATCTCAACACG
MXA	ATCCTGGGATTTTGGGGC TT	CCGCTTGTCGCTGGTGTCG
OAS1	AGGAAAGGTGCTTCCGAGGTAG	GGACTGAGGAAGACAACCAGGT

Figure legends

Figure 1: **UPRmt induction by GTPP is ATF5-dependent and associated with early stress granule (SG) formation**. (**A**) U2OS cells were transfected with non-targeting siRNA (siCont) or ATF5-specifc siRNA (siATF5), after 48 h cells were treated either with DMSO or 10 µM GTPP for 4h and mRNA levels of UPRmt markers were measured by RT-qPCR. Results shown as mean ± SD, n=3, normalised to RPL9 mRNA and shown relative to siCont DMSO expression level, analysed by two-way ANOVA (****, P < 0.0001; ***, P < 0.001; **, P < 0.01; *, P < 0.05). (**B**) Cells were treated with GTPP up to 8 h and analysed by immunofluorescence for the SG markers G3BP1 (cyan) and eIF3η (magenta). Nuclei were stained with DAPI. Scale bars indicate 10 µm. (**C**) Quantification by manual counting of cells with SGs

using ImageJ, at least 100 cells were counted per replicate. Results are shown as mean ± SD, n=3 and were analysed by one-way ANOVA compared to DMSO treated cells (****, P < 0.0001; *, P < 0.05).

Figure 2: UPRmt activation by GTPP results in activation of the integrated stress response (ISR) through PERK. (**A**) Western blot analysis of ATF4, GADD34 and p-eIF2α expression levels after GTPP treatment up to 6 h. Representative blot of three independent experiments, with molecular weights (kDa) indicated on the left and antibodies used on the right. Band quantifications were normalised to GAPDH and relative to DMSO for each time point. (**B**) RT-qPCR analysis of ATF4, ATF5, CHOP and GADD34 mRNA expression followed by GTPP treatment up to 6 h. Results shown as mean ± SD, n=3, normalised to RPL9 mRNA and shown relative to DMSO expression level, analysed by one-way ANOVA (****, P < 0.0001; *, P < 0.05). (**C**) Cells were treated with GTPP for 2 h or transfected with dsRNA (positive control) and analysed by immunofluorescence with anti-dsRNA and the mitochondrial marker anti-TOMM20. Nucleus stained with DAPI. Scale bars indicate 10 µm. (**D**) RT-qPCR analysis of IFN-stimulated genes including CXCL10, CCL5, MX1 and OAS1 after 1, 4 and 8 h GTPP exposure. Results shown as mean ± SD, n=3, normalised to RPL9 mRNA and shown relative to DMSO expression level. (**E**) Cells were treated with either DMSO, 0.1 µM PERK inhibitor GSK2606414 or 1 µM GCN2 inhibitor A-92 for 1 h followed by treated with 10 µM GTPP for 2h, 5 mM DTT for 2h and 2h-post UV light exposure at 20mJ/cm^3. Shown is a representative blot from three independent experiments. Band quantifications were normalised to GAPDH and relative to DMSO for each inhibitor used.

Figure 3: Pre-treatment with UPRmt inducers impairs assembly of eIF2α-dependent SGs and prevents eIF2α phosphorylation. (**A**) Top right; schematic diagram of the experimental setup. U2OS cells were pre-treated with 10 µM GTPP (**A**) or 0.5 mM paraquat (Pq) (**D**) and 0.5 mM sodium arsenite (Ars) was added 30 min before harvest and cells were analysed by immunofluorescence for the SG markers G3BP1 (cyan) and eIF3η (magenta). Nuclei were stained with DAPI. Scale bars indicate 10 µm. (**B, E**) Panels show quantification by manual counting of cells with SGs using ImageJ, at least 100 cells were counted per replicate. Results are shown as mean ± SD, n=3 and were analysed by one-way ANOVA (****, P < 0.0001; ***, P < 0.001; *, P < 0.05). (**C, F**) Representative western blot analysis of three independent experiments of Ars-induced eIF2α phosphorylation levels in U2OS cells pre-treated with GTPP (C) and Pq (D). eIF2α phosphorylation levels were normalized to GAPDH expression levels and are shown as relative to DMSO/NT cells; NT, non-treated. (**G**) Scatter plot displaying the average size of SGs (left) and the number of SGs per cell in cells (right) of data from D using Analyze Particle plugin from ImageJ. Each point represents individual cells analysed from three independent experiments (100 cells per condition) and were analysed by Mann-Whitney test (****, P < 0.0001).

Figure 4: GADD34 upregulation is responsible for preventing eIF2α-phosphorylation and SG assembly. U2OS control (Ctrl) or GADD34 KO cells were treated with GTPP 4 h (**A**) or paraquat (Pq) 48 h (**C**) and 0.5 mM sodium arsenite (Ars) was added 30 min before harvest and cells were analysed by immunofluorescence for the SG markers G3BP1 (cyan) and eIF3η (magenta). Nucleus stained with DAPI. Scale bars indicate 10 µm. (**B, D**) Panels show quantification by manual counting of cells with SGs using ImageJ, at least 100 cells were counted per replicate. Results are shown as mean ± SD, n=3 and were analysed by two-way ANOVA (****, P < 0.0001; **, P < 0.01). (**F, G**) Representative

western blot analysis of three independent experiments of same conditions as above showing GADD34 protein levels and arsenite-induced eIF2α phosphorylation levels in Ctrl and GADD34 U2OS cells pre-treated with GTPP (**F**) and Pq (**G**). eIF2α phosphorylation levels were normalized to eIF3A or GAPDH expression levels and are shown as relative to DMSO/NT cells; NT, non-treated.

Figure 5: UPRmt activation also alters eIF2α-independent SG formation associated with an upregulation of SG disassembly chaperones. U2OS were pre-treated with 10 μM GTPP (**A**) or 0.5 mM paraquat (Pq) (**C**) and 2 μM silvestrol (Silv) was added 1 h before harvest, analysed by immunofluorescence for the SG markers G3BP1 (cyan) and eIF3η (magenta). Nucleus stained with DAPI. Scale bars indicate 10 μm. (**B, D**) Panels show quantification by manual counting of cells with SG using ImageJ, at least 100 cells were counted per replicate. Results are shown as mean ± SD, n=3, and were analysed by one-way ANOVA (****, P < 0.0001; ns, non-significant). (**E**) Scatter plot displaying the average size of SGs (left) and the number of SGs per cell in cells (right) of data from D using G3BP1 channel and Analyze Particle plugin from ImageJ. Each point represents individual cells analysed from three independent experiments (100 cells per condition) and were analysed by Mann-Whitney test (****, P < 0.0001). (**F, G**) RT-qPCR analysis of SG disassembly chaperones HSP90AA1, HSP90AB1 and DYRK3 mRNA expression levels in response to GTPP (**F**) and Pq (**G**) treatment. Results shown as mean ± SD, n=3, normalised to RpL9 mRNA and shown relative to DMSO/NT expression level, analysed by two-way ANOVA (****, P < 0.0001; **, P < 0.01; *, P < 0.05).

Figure 6: Presence of SGs perturbs mitochondrial respiration during UPRmt. (**A**) Schematic diagram of the respiratory profile of live cells using Seahorse Cell Mito Stress Test, showing the key parameters of mitochondrial function and the drugs being used. Briefly, oxygen consumption rate is measured when cells are sequentially stimulated with oligomycin (ATP synthase inhibitor), FCCP (protonophore, uncoupling) and antimycin A/rotenone (inhibitors of complex III and I). (**B**) Representative respiratory profile of three independent experiments of WT (solid line) and G3BP1/2 dKO (dashed line) U2OS cells treated with DMSO (black) or GTPP (purple) for 2 h. (**C**) Various parameters of mitochondrial respiration were analysed based on data of B. Results shown as mean ± SD, n=3 and as fold change to DMSO-treated cells for each cell line, analysed by two-way ANOVA (****, P < 0.0001; ***, P < 0.001; **, P < 0.01; *, P < 0.05).

Supplementary Figure 1: UPRmt activation by paraquat in U2OS cells. RT-qPCR analysis of ISR and UPRmt markers followed by 0.5 mM paraquat treatment for 48 h. Results shown as mean ± SD, n=3, normalised to RPL9 mRNA and shown relative to NT expression level, analysed by two-way ANOVA (****, P < 0.0001; *, P < 0.05); NT, non-treated.

Supplementary Figure 2: ATF5-depedent transcriptional programme is not responsible for regulating SG dynamics. (**A**) U2OS cells were transfected with non-targeting siRNA (siCont) or ATF5-specifc siRNA (siATF5), after 48 h cells were treated with GTPP 4h and sodium arsenite (Ars) was added 30 min before harvesting and cells were analysed by immunofluorescence for the SG markers G3BP1 (cyan) and eIF3η (magenta). Nucleus stained with DAPI. Scale bars indicate 10 μm. (**B**) Panel shows quantification by manual counting of cells with SGs using ImageJ, at least 100 cells were counted

per replicate. Results are shown as mean ± SD, n=3 and were analysed by two-way ANOVA (ns, non-significant).

Supplementary Figure 3: Validation of U2OS GADD34 KO single cell clones by Western blot. Clones were treated with 2 µM thapsigargin (Thap) or with DMSO (-) for 3 h and GADD34 protein levels were analysed by western blot. eIF3A was used as loading control.

Supplementary Figure 4: U2OS G3BP1/2 dKO cells do not form SGs. U2OS WT and G3BP1/2 dKO cells were treated with arsenite (Ars) for 30 min and analysed by immunofluorescence using the SG markers G3BP1 (cyan) and eIF3η (magenta). Nuclei were stained with DAPI. Scale bars indicate 10 µm.

Data availability Statement

All the data are included in the article. All unique reagents generated in this study are available from the corresponding authors with a completed Materials Transfer Agreement.

Acknowledgments

We thank P. J. McCormick (Queen Mary University London) for helpful discussions during the study.

Author contributions

N. L., A. R. and I. S. conceptualization; N. L., M. L-N., A. R., Z. S., R. S. and I. S. methodology; N. L., M. L-N., A. R., and Z. S. formal analysis; N. L., M. L-N., A. R., Z. S., R. S. and I. S. investigation; N. L. and M. L-N. writing–original draft; N. L., M. L-N., A. R., Z. S., R. S. and I. S. writing–review & editing; N.L. supervision. N. L., A. R., and I. S. funding acquisition.

Funding and additional information

Work in N.L.'s laboratory is supported by a Biotechnology and Biological Sciences Research Council research grant [BB/V014528/1]. M. L-N. and R. S. are supported by DCSA4 Ph.D studentships from the University of Surrey. Work in A.R.'s laboratory was supported by the Deutsche Forschungsgemeinschaft (DFG, German Research Foundation) project numbers 240245660 SFB1129 TP13 and 278001972 TRR186 A14.

Conflict of interest

The authors declare that they have no conflicts of interest with the contents of this article.

References

Almeida, L.M., B.R. Pinho, M.R. Duchen, and J.M.A. Oliveira. 2022. The PERKs of mitochondria protection during stress: insights for PERK modulation in neurodegenerative and metabolic diseases. *Biol Rev Camb Philos Soc*. 97:1737-1748.

Amen, T., and D. Kaganovich. 2021. Stress granules inhibit fatty acid oxidation by modulating mitochondrial permeability. *Cell Rep*. 35:109237.

Anderson, N.S., and C.M. Haynes. 2020. Folding the Mitochondrial UPR into the Integrated Stress Response. *Trends Cell Biol*. 30:428-439.

Anderson, P., N. Kedersha, and P. Ivanov. 2015. Stress granules, P-bodies and cancer. *Biochim Biophys Acta*. 1849:861-870.

Aoyama-Ishiwatari, S., T. Okazaki, S.I. Iemura, T. Natsume, Y. Okada, and Y. Gotoh. 2021. NUDT21 Links Mitochondrial IPS-1 to RLR-Containing Stress Granules and Activates Host Antiviral Defense. *J Immunol*. 206:154-163.

Arimoto, K., H. Fukuda, S. Imajoh-Ohmi, H. Saito, and M. Takekawa. 2008. Formation of stress granules inhibits apoptosis by suppressing stress-responsive MAPK pathways. *Nat Cell Biol*. 10:1324-1332.

Aulas, A., M.M. Fay, S.M. Lyons, C.A. Achorn, N. Kedersha, P. Anderson, and P. Ivanov. 2017. Stress-specific differences in assembly and composition of stress granules and related foci. *J Cell Sci*. 130:927-937.

Baker, B.M., A.M. Nargund, T. Sun, and C.M. Haynes. 2012. Protective coupling of mitochondrial function and protein synthesis via the eIF2α kinase GCN-2. *PLoS Genet*. 8:e1002760.

Banoth, B., and S.L. Cassel. 2018. Mitochondria in innate immune signaling. *Transl Res*. 202:52-68.

Baron, D.M., L.J. Kaushansky, C.L. Ward, R.R. Sama, R.J. Chian, K.J. Boggio, A.J. Quaresma, J.A. Nickerson, and D.A. Bosco. 2013. Amyotrophic lateral sclerosis-linked FUS/TLS alters stress granule assembly and dynamics. *Mol Neurodegener*. 8:30.

Begovich, K., A.Q. Vu, G. Yeo, and J.E. Wilhelm. 2020. Conserved metabolite regulation of stress granule assembly via AdoMet. *J Cell Biol*. 219.

Bordeleau, M.E., F. Robert, B. Gerard, L. Lindqvist, S.M. Chen, H.G. Wendel, B. Brem, H. Greger, S.W. Lowe, J.A. Porco, Jr., and J. Pelletier. 2008. Therapeutic suppression of translation initiation modulates chemosensitivity in a mouse lymphoma model. *J Clin Invest*. 118:2651-2660.

Brostrom, C.O., C.R. Prostko, R.J. Kaufman, and M.A. Brostrom. 1996. Inhibition of translational initiation by activators of the glucose-regulated stress protein and heat shock protein stress response systems. Role of the interferon-inducible double-stranded RNA-activated eukaryotic initiation factor 2alpha kinase. *J Biol Chem*. 271:24995-25002.

Burke, J.M., E.T. Lester, D. Tauber, and R. Parker. 2020. RNase L promotes the formation of unique ribonucleoprotein granules distinct from stress granules. *J Biol Chem*. 295:1426-1438.

Cereghetti, G., C. Wilson-Zbinden, V.M. Kissling, M. Diether, A. Arm, H. Yoo, I. Piazza, S. Saad, P. Picotti, D.A. Drummond, U. Sauer, R. Dechant, and M. Peter. 2021. Reversible amyloids of pyruvate kinase couple cell metabolism and stress granule disassembly. *Nat Cell Biol*. 23:1085-1094.

Chamseddine, D., S.A. Mahmud, A.K. Westfall, T.A. Castoe, R.E. Berg, and M.W. Pellegrino. 2022. The mitochondrial UPR regulator ATF5 promotes intestinal barrier function via control of the satiety response. *Cell Rep*. 41:111789.

Chen, W., H. Zhao, and Y. Li. 2023. Mitochondrial dynamics in health and disease: mechanisms and potential targets. *Signal Transduction and Targeted Therapy*. 8:333.

Cocheme, H.M., and M.P. Murphy. 2008. Complex I is the major site of mitochondrial superoxide production by paraquat. *J Biol Chem*. 283:1786-1798.

Corbet, G.A., and R. Parker. 2019. RNP Granule Formation: Lessons from P-Bodies and Stress Granules. *Cold Spring Harb Symp Quant Biol*. 84:203-215.

D'Souza, A.R., and M. Minczuk. 2018. Mitochondrial transcription and translation: overview. *Essays Biochem*. 62:309-320.

Deng, J., H.P. Harding, B. Raught, A.C. Gingras, J.J. Berlanga, D. Scheuner, R.J. Kaufman, D. Ron, and N. Sonenberg. 2002. Activation of GCN2 in UV-irradiated cells inhibits translation. *Curr Biol*. 12:1279-1286.

Dever, T.E., L. Feng, R.C. Wek, A.M. Cigan, T.F. Donahue, and A.G. Hinnebusch. 1992. Phosphorylation of initiation factor 2 alpha by protein kinase GCN2 mediates gene-specific translational control of GCN4 in yeast. *Cell*. 68:585-596.

Donehower, L.A., T. Soussi, A. Korkut, Y. Liu, A. Schultz, M. Cardenas, X. Li, O. Babur, T.K. Hsu, O. Lichtarge, J.N. Weinstein, R. Akbani, and D.A. Wheeler. 2019. Integrated Analysis of TP53 Gene and Pathway Alterations in The Cancer Genome Atlas. *Cell Rep*. 28:1370-1384.e1375.

Eiermann, N., K. Haneke, Z. Sun, G. Stoecklin, and A. Ruggieri. 2020. Dance with the Devil: Stress Granules and Signaling in Antiviral Responses. *Viruses*. 12.

Fiorese, C.J., A.M. Schulz, Y.-F. Lin, N. Rosin, M.W. Pellegrino, and C.M. Haynes. 2016. The Transcription Factor ATF5 Mediates a Mammalian Mitochondrial UPR. *Curr Biol*. 26:2037-2043.

Fu, Y., O. Sacco, E. DeBitetto, E. Kanshin, B. Ueberheide, and A. Sfeir. 2023. Mitochondrial DNA breaks activate an integrated stress response to reestablish homeostasis. *Mol Cell*.

Fujikawa, D., T. Nakamura, D. Yoshioka, Z. Li, H. Moriizumi, M. Taguchi, N. Tokai-Nishizumi, H. Kozuka-Hata, M. Oyama, and M. Takekawa. 2023. Stress granule formation inhibits stress-induced apoptosis by selectively sequestering executioner caspases. *Curr Biol*. 33:1967-1981.e1968.

Giorgi, C., S. Marchi, and P. Pinton. 2018. The machineries, regulation and cellular functions of mitochondrial calcium. *Nat Rev Mol Cell Biol*. 19:713-730.

Guo, X., G. Aviles, Y. Liu, R. Tian, B.A. Unger, Y.T. Lin, A.P. Wiita, K. Xu, M.A. Correia, and M. Kampmann. 2020. Mitochondrial stress is relayed to the cytosol by an OMA1-DELE1-HRI pathway. *Nature*. 579:427-432.

Harding, H.P., I. Novoa, Y. Zhang, H. Zeng, R. Wek, M. Schapira, and D. Ron. 2000. Regulated translation initiation controls stress-induced gene expression in mammalian cells. *Mol Cell*. 6:1099-1108.

Harding, H.P., Y. Zhang, H. Zeng, I. Novoa, P.D. Lu, M. Calfon, N. Sadri, C. Yun, B. Popko, R. Paules, D.F. Stojdl, J.C. Bell, T. Hettmann, J.M. Leiden, and D. Ron. 2003. An integrated stress response regulates amino acid metabolism and resistance to oxidative stress. *Mol Cell*. 11:619-633.

Hofmann, S., N. Kedersha, P. Anderson, and P. Ivanov. 2020. Molecular mechanisms of stress granule assembly and disassembly. *Biochim Biophys Acta Mol Cell Res*:118876.

Houtkooper, R.H., L. Mouchiroud, D. Ryu, N. Moullan, E. Katsyuba, G. Knott, R.W. Williams, and J. Auwerx. 2013. Mitonuclear protein imbalance as a conserved longevity mechanism. *Nature*. 497:451-457.

Jain, S., J.R. Wheeler, R.W. Walters, A. Agrawal, A. Barsic, and R. Parker. 2016. ATPase-Modulated Stress Granules Contain a Diverse Proteome and Substructure. *Cell*. 164:487-498.

Jiang, D., H. Cui, N. Xie, S. Banerjee, R.M. Liu, H. Dai, V.J. Thannickal, and G. Liu. 2020. ATF4 Mediates Mitochondrial Unfolded Protein Response in Alveolar Epithelial Cells. *Am J Respir Cell Mol Biol*. 63:478-489.

Kang, B.H., J. Plescia, H.Y. Song, M. Meli, G. Colombo, K. Beebe, B. Scroggins, L. Neckers, and D.C. Altieri. 2009. Combinatorial drug design targeting multiple cancer signaling networks controlled by mitochondrial Hsp90. *J Clin Invest*. 119:454-464.

Kaspar, S., C. Oertlin, K. Szczepanowska, A. Kukat, K. Senft, C. Lucas, S. Brodesser, M. Hatzoglou, O. Larsson, I. Topisirovic, and A. Trifunovic. 2021. Adaptation to mitochondrial stress requires CHOP-directed tuning of ISR. *Sci Adv*. 7.

Kedersha, N., S. Chen, N. Gilks, W. Li, I.J. Miller, J. Stahl, and P. Anderson. 2002. Evidence that ternary complex (eIF2-GTP-tRNA(i)(Met))-deficient preinitiation complexes are core constituents of mammalian stress granules. *Mol Biol Cell*. 13:195-210.

Kim, Y., J. Park, S. Kim, M. Kim, M.G. Kang, C. Kwak, M. Kang, B. Kim, H.W. Rhee, and V.N. Kim. 2018. PKR Senses Nuclear and Mitochondrial Signals by Interacting with Endogenous Double-Stranded RNAs. *Mol Cell*. 71:1051-1063.e1056.

Kitajima, H., R. Maruyama, T. Niinuma, E. Yamamoto, A. Takasawa, K. Takasawa, K. Ishiguro, A. Tsuyada, R. Suzuki, G. Sudo, T. Kubo, K. Mitsuhashi, M. Idogawa, S. Tange, M. Toyota, A. Yoshido, K. Kumegawa, M. Kai, K. Yanagihara, T. Tokino, M. Osanai, H. Nakase, and H. Suzuki. 2023. TM4SF1-AS1 inhibits apoptosis by promoting stress granule formation in cancer cells. *Cell Death Dis*. 14:424.

Klein, P., S.M. Kallenberger, H. Roth, K. Roth, T.B.N. Ly-Hartig, V. Magg, J. Ales, S.R. Talemi, Y. Qiang, S. Wolf, O. Oleksiuk, R. Kurilov, B. Di Ventura, R. Bartenschlager, R. Eils, K. Rohr, F.A. Hamprecht, T. Hofer, O.T. Fackler, G. Stoecklin, and A. Ruggieri. 2022. Temporal control of the integrated stress response by a stochastic molecular switch. *Sci Adv*. 8:eabk2022.

Lee, J.E., P.I. Cathey, H. Wu, R. Parker, and G.K. Voeltz. 2020. Endoplasmic reticulum contact sites regulate the dynamics of membraneless organelles. *Science*. 367.

Lee, Y.Y., R.C. Cevallos, and E. Jan. 2009. An Upstream Open Reading Frame Regulates Translation of GADD34 during Cellular Stresses That Induce eIF2α Phosphorylation*. *Journal of Biological Chemistry*. 284:6661 - 6673.

Liao, Y.C., M.S. Fernandopulle, G. Wang, H. Choi, L. Hao, C.M. Drerup, R. Patel, S. Qamar, J. Nixon-Abell, Y. Shen, W. Meadows, M. Vendruscolo, T.P.J. Knowles, M. Nelson, M.A. Czekalska, G. Musteikyte, M.A. Gachechiladze, C.A. Stephens, H.A. Pasolli, L.R. Forrest, P. St George-Hyslop, J.

Lippincott-Schwartz, and M.E. Ward. 2019. RNA Granules Hitchhike on Lysosomes for Long-Distance Transport, Using Annexin A11 as a Molecular Tether. *Cell*. 179:147-164.e120.

Livak, K.J., and T.D. Schmittgen. 2001. Analysis of relative gene expression data using real-time quantitative PCR and the 2(-Delta Delta C(T)) Method. *Methods*. 25:402-408.

Mahmud, S.A., M.A. Qureshi, M. Sapkota, and M.W. Pellegrino. 2020. A pathogen branched-chain amino acid catabolic pathway subverts host survival by impairing energy metabolism and the mitochondrial UPR. *PLoS Pathog*. 16:e1008918.

Martinus, R.D., G.P. Garth, T.L. Webster, P. Cartwright, D.J. Naylor, P.B. Høj, and N.J. Hoogenraad. 1996. Selective induction of mitochondrial chaperones in response to loss of the mitochondrial genome. *Eur J Biochem*. 240:98-103.

Matheny, T., B.S. Rao, and R. Parker. 2019. Transcriptome-Wide Comparison of Stress Granules and P-Bodies Reveals that Translation Plays a Major Role in RNA Partitioning. *Mol Cell Biol*. 39.

Mediani, L., F. Antoniani, V. Galli, J. Vinet, A.D. Carrà, I. Bigi, V. Tripathy, T. Tiago, M. Cimino, G. Leo, T. Amen, D. Kaganovich, C. Cereda, O. Pansarasa, J. Mandrioli, P. Tripathi, D. Troost, E. Aronica, J. Buchner, A. Goswami, J. Sterneckert, S. Alberti, and S. Carra. 2021. Hsp90-mediated regulation of DYRK3 couples stress granule disassembly and growth via ^{mt}ORC1 signaling. *EMBO reports*. 22:e51740.

Münch, C., and J.W. Harper. 2016. Mitochondrial unfolded protein response controls matrix pre-RNA processing and translation. *Nature*. 534:710-713.

Munkácsy, E., and S.L. Rea. 2014. The paradox of mitochondrial dysfunction and extended longevity. *Exp Gerontol*. 56:221-233.

Namkoong, S., A. Ho, Y.M. Woo, H. Kwak, and J.H. Lee. 2018. Systematic Characterization of Stress-Induced RNA Granulation. *Mol Cell*. 70:175-187 e178.

Nargund, A.M., M.W. Pellegrino, C.J. Fiorese, B.M. Baker, and C.M. Haynes. 2012. Mitochondrial import efficiency of ATFS-1 regulates mitochondrial UPR activation. *Science*. 337:587-590.

Norat, P., S. Soldozy, J.D. Sokolowski, C.M. Gorick, J.S. Kumar, Y. Chae, K. Yağmurlu, F. Prada, M. Walker, M.R. Levitt, R.J. Price, P. Tvrdik, and M.Y.S. Kalani. 2020. Mitochondrial dysfunction in neurological disorders: Exploring mitochondrial transplantation. *npj Regenerative Medicine*. 5:22.

Novoa, I., H. Zeng, H.P. Harding, and D. Ron. 2001. Feedback inhibition of the unfolded protein response by GADD34-mediated dephosphorylation of eIF2alpha. *J Cell Biol*. 153:1011-1022.

Paget, M., C. Cadena, S. Ahmad, H.T. Wang, T.X. Jordan, E. Kim, B. Koo, S.M. Lyons, P. Ivanov, B. tenOever, X. Mu, and S. Hur. 2023. Stress granules are shock absorbers that prevent excessive innate immune responses to dsRNA. *Mol Cell*. 83:1180-1196.e1188.

Park, J.Y., and O.S. Shin. 2023. Stress Granules Inhibit Coxsackievirus B3-Mediated Cell Death via Reduction of Mitochondrial Reactive Oxygen Species and Viral Extracellular Release. *J Microbiol Biotechnol*. 33:582-590.

Pellegrino, M.W., A.M. Nargund, N.V. Kirienko, R. Gillis, C.J. Fiorese, and C.M. Haynes. 2014. Mitochondrial UPR-regulated innate immunity provides resistance to pathogen infection. *Nature*. 516:414-417.

Pindel, A., and A. Sadler. 2011. The role of protein kinase R in the interferon response. *J Interferon Cytokine Res*. 31:59-70.

Quirós, P.M., A. Mottis, and J. Auwerx. 2016. Mitonuclear communication in homeostasis and stress. *Nat Rev Mol Cell Biol*. 17:213-226.

Quirós, P.M., M.A. Prado, N. Zamboni, D. D'Amico, R.W. Williams, D. Finley, S.P. Gygi, and J. Auwerx. 2017. Multi-omics analysis identifies ATF4 as a key regulator of the mitochondrial stress response in mammals. *J Cell Biol*. 216:2027-2045.

Radetskyy, R., A. Daher, and A. Gatignol. 2018. ADAR1 and PKR, interferon stimulated genes with clashing effects on HIV-1 replication. *Cytokine Growth Factor Rev*. 40:48-58.

Reineke, L.C., S.A. Cheema, J. Dubrulle, and J.R. Neilson. 2018. Chronic starvation induces noncanonical pro-death stress granules. *J Cell Sci*. 131.

Reineke, L.C., and J.R. Neilson. 2019. Differences between acute and chronic stress granules, and how these differences may impact function in human disease. *Biochem Pharmacol*. 162:123-131.

Repici, M., M. Hassanjani, D.C. Maddison, P. Garcao, S. Cimini, B. Patel, E.M. Szego, K.R. Straatman, K.S. Lilley, T. Borsello, T.F. Outeiro, L. Panman, and F. Giorgini. 2019. The Parkinson's Disease-Linked Protein DJ-1 Associates with Cytoplasmic mRNP Granules During Stress and Neurodegeneration. *Mol Neurobiol*. 56:61-77.

Rolland, S.G., S. Schneid, M. Schwarz, E. Rackles, C. Fischer, S. Haeussler, S.G. Regmi, A. Yeroslaviz, B. Habermann, D. Mokranjac, E. Lambie, and B. Conradt. 2019. Compromised Mitochondrial Protein Import Acts as a Signal for UPR(^{mt}). *Cell Rep*. 28:1659-1669.e1655.

Rollins, M., S. Huard, A. Morettin, J. Takuski, T.T. Pham, M.D. Fullerton, J. Côté, and K. Baetz. 2017. Lysine acetyltransferase NuA4 and acetyl-CoA regulate glucose-deprived stress granule formation in Saccharomyces cerevisiae. *PLoS Genet*. 13:e1006626.

Ron, D. 2002. Translational control in the endoplasmic reticulum stress response. *J Clin Invest*. 110:1383-1388.

Saad, S., G. Cereghetti, Y. Feng, P. Picotti, M. Peter, and R. Dechant. 2017. Reversible protein aggregation is a protective mechanism to ensure cell cycle restart after stress. *Nat Cell Biol*. 19:1202-1213.

Samluk, L., M. Urbanska, K. Kisielewska, K. Mohanraj, M.J. Kim, K. Machnicka, E. Liszewska, J. Jaworski, and A. Chacinska. 2019. Cytosolic translational responses differ under conditions of severe short-term and long-term mitochondrial stress. *Mol Biol Cell*. 30:1864-1877.

Schwed-Gross, A., H. Hamiel, G.P. Faber, M. Angel, R. Ben-Yishay, J.I.C. Benichou, D. Ishay-Ronen, and Y. Shav-Tal. 2022. Glucocorticoids enhance chemotherapy-driven stress granule assembly and impair granule dynamics, leading to cell death. *J Cell Sci*. 135.

Smyrnias, I., S.P. Gray, D.O. Okonko, G. Sawyer, A. Zoccarato, N. Catibog, B. López, A. González, S. Ravassa, J. Díez, and A.M. Shah. 2019. Cardioprotective Effect of the Mitochondrial Unfolded Protein Response During Chronic Pressure Overload. *J Am Coll Cardiol*. 73:1795-1806.

Sorrentino, V., M. Romani, L. Mouchiroud, J.S. Beck, H. Zhang, D. D'Amico, N. Moullan, F. Potenza, A.W. Schmid, S. Rietsch, S.E. Counts, and J. Auwerx. 2017. Enhancing mitochondrial proteostasis reduces amyloid-β proteotoxicity. *Nature*. 552:187-193.

Spinelli, J.B., and M.C. Haigis. 2018. The multifaceted contributions of mitochondria to cellular metabolism. *Nat Cell Biol*. 20:745-754.

Suomalainen, A., and B.J. Battersby. 2018. Mitochondrial diseases: the contribution of organelle stress responses to pathology. *Nat Rev Mol Cell Biol*. 19:77-92.

Sutandy, F.X.R., I. Gößner, G. Tascher, and C. Münch. 2023. A cytosolic surveillance mechanism activates the mitochondrial UPR. *Nature*. 618:849-854.

Takahashi, M., M. Higuchi, H. Matsuki, M. Yoshita, T. Ohsawa, M. Oie, and M. Fujii. 2013. Stress granules inhibit apoptosis by reducing reactive oxygen species production. *Mol Cell Biol*. 33:815-829.

Tauber, D., G. Tauber, A. Khong, B. Van Treeck, J. Pelletier, and R. Parker. 2020. Modulation of RNA Condensation by the DEAD-Box Protein eIF4A. *Cell*. 180:411-426 e416.

Vanderweyde, T., H. Yu, M. Varnum, L. Liu-Yesucevitz, A. Citro, T. Ikezu, K. Duff, and B. Wolozin. 2012. Contrasting pathology of the stress granule proteins TIA-1 and G3BP in tauopathies. *J Neurosci*. 32:8270-8283.

Wang, J., J.M. Choi, A.S. Holehouse, H.O. Lee, X. Zhang, M. Jahnel, S. Maharana, R. Lemaitre, A. Pozniakovsky, D. Drechsel, I. Poser, R.V. Pappu, S. Alberti, and A.A. Hyman. 2018. A Molecular Grammar Governing the Driving Forces for Phase Separation of Prion-like RNA Binding Proteins. *Cell*. 174:688-699 e616.

Wang, T., X. Tian, H.B. Kim, Y. Jang, Z. Huang, C.H. Na, and J. Wang. 2022a. Intracellular energy controls dynamics of stress-induced ribonucleoprotein granules. *Nat Commun*. 13:5584.

Wang, Y.T., Y. Lim, M.N. McCall, K.T. Huang, C.M. Haynes, K. Nehrke, and P.S. Brookes. 2019. Cardioprotection by the mitochondrial unfolded protein response requires ATF5. *Am J Physiol Heart Circ Physiol*. 317:H472-H478.

Wang, Z., H. Bo, Y. Song, C. Li, and Y. Zhang. 2022b. Mitochondrial ROS Produced by Skeletal Muscle Mitochondria Promote the Decisive Signal for UPRmt Activation. *Biomed Res Int*. 2022:7436577.

Wek, R.C., H.Y. Jiang, and T.G. Anthony. 2006. Coping with stress: eIF2 kinases and translational control. *Biochem Soc Trans*. 34:7-11.

Wheeler, J.R., T. Matheny, S. Jain, R. Abrisch, and R. Parker. 2016. Distinct stages in stress granule assembly and disassembly. *Elife*. 5.

Wippich, F., B. Bodenmiller, M.G. Trajkovska, S. Wanka, R. Aebersold, and L. Pelkmans. 2013. Dual specificity kinase DYRK3 couples stress granule condensation/dissolution to ^{mt}ORC1 signaling. *Cell*. 152:791-805.

Wolozin, B., and P. Ivanov. 2019. Stress granules and neurodegeneration. *Nat Rev Neurosci*. 20:649-666.

Yang, P., C. Mathieu, R.M. Kolaitis, P. Zhang, J. Messing, U. Yurtsever, Z. Yang, J. Wu, Y. Li, Q. Pan, J. Yu, E.W. Martin, T. Mittag, H.J. Kim, and J.P. Taylor. 2020. G3BP1 Is a Tunable Switch that Triggers Phase Separation to Assemble Stress Granules. *Cell*. 181:325-345.e328.

Yoo, H., C. Triandafillou, and D.A. Drummond. 2019. Cellular sensing by phase separation: Using the process, not just the products. *J Biol Chem*. 294:7151-7159.

Zhang, S., A. Macias-Garcia, J. Velazquez, E. Paltrinieri, R.J. Kaufman, and J.J. Chen. 2018. HRI coordinates translation by eIF2αP and mTORC1 to mitigate ineffective erythropoiesis in mice during iron deficiency. *Blood*. 131:450-461.

Zhao, Q., J. Wang, I.V. Levichkin, S. Stasinopoulos, M.T. Ryan, and N.J. Hoogenraad. 2002. A mitochondrial specific stress response in mammalian cells. *Embo j*. 21:4411-4419.

Zhou, Z., J. Lu, M. Yang, J. Cai, Q. Fu, J. Ma, and L. Zhu. 2022. The mitochondrial unfolded protein response (UPR(^{mt})) protects against osteoarthritis. *Exp Mol Med*. 54:1979-1990.

Figure 1

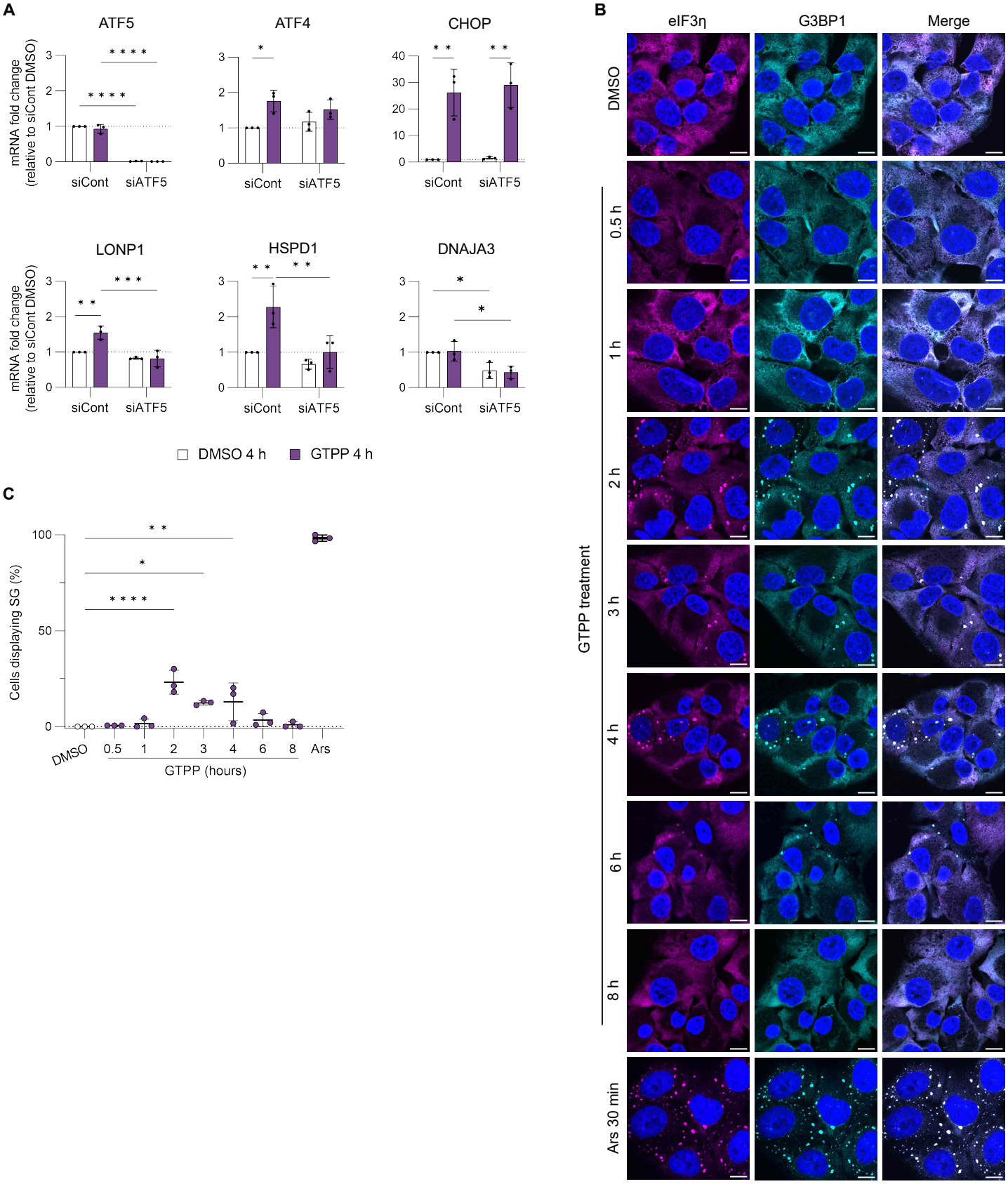
A
ATF5
ATF4
CHOP
LONP1
HSPD1
DNAJA3
mRNA fold change (relative to siCont DMSO)
siCont
siATF5
DMSO 4 h
GTPP 4 h
B
eIF3η
G3BP1
Merge
DMSO
0.5 h
1 h
2 h
3 h
4 h
6 h
8 h
Ars 30 min
GTPP treatment
C
Cells displaying SG (%)
DMSO
0.5
1
2
3
4
6
8
Ars
GTPP (hours)

Figure 2

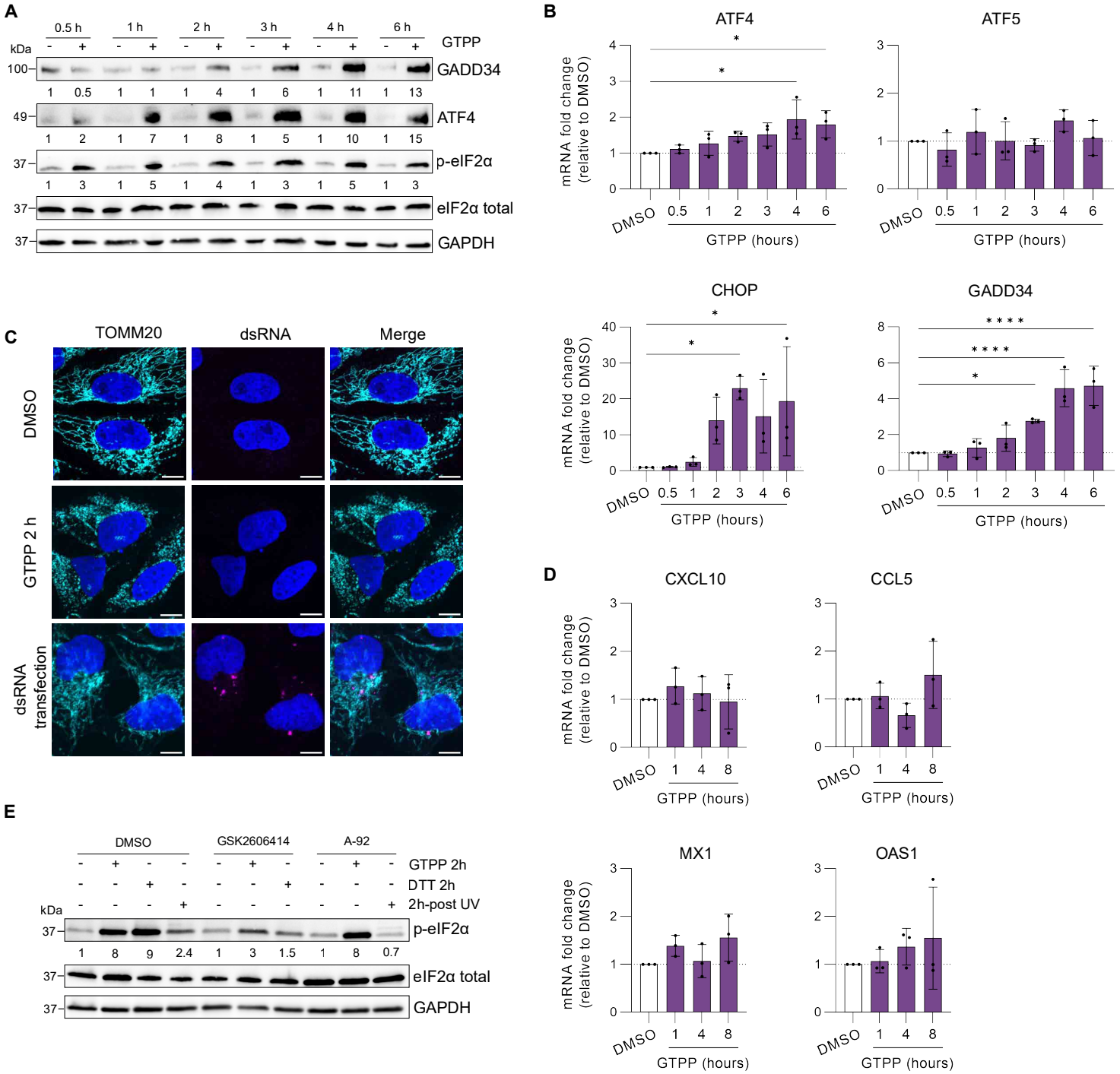
A
0.5 h
1 h
2 h
3 h
4 h
6 h
GTPP
kDa
100
GADD34
1 0.5 1 1 1 4 1 6 1 11 1 13
49
ATF4
1 2 1 7 1 8 1 5 1 10 1 15
37
p-eIF2α
1 3 1 5 1 4 1 3 1 5 1 3
37
eIF2α total
37
GAPDH
B
ATF4
ATF5
CHOP
GADD34
mRNA fold change (relative to DMSO)
DMSO
0.5
1
2
3
4
6
GTPP (hours)
C
TOMM20
dsRNA
Merge
DMSO
GTPP 2 h
dsRNA transfection
D
CXCL10
CCL5
MX1
OAS1
mRNA fold change (relative to DMSO)
DMSO
1
4
8
GTPP (hours)
E
DMSO
GSK2606414
A-92
GTPP 2h
DTT 2h
2h-post UV
kDa
37
p-eIF2α
1 8 9 2.4 1 3 1.5 1 8 0.7
37
eIF2α total
37
GAPDH

Figure 3

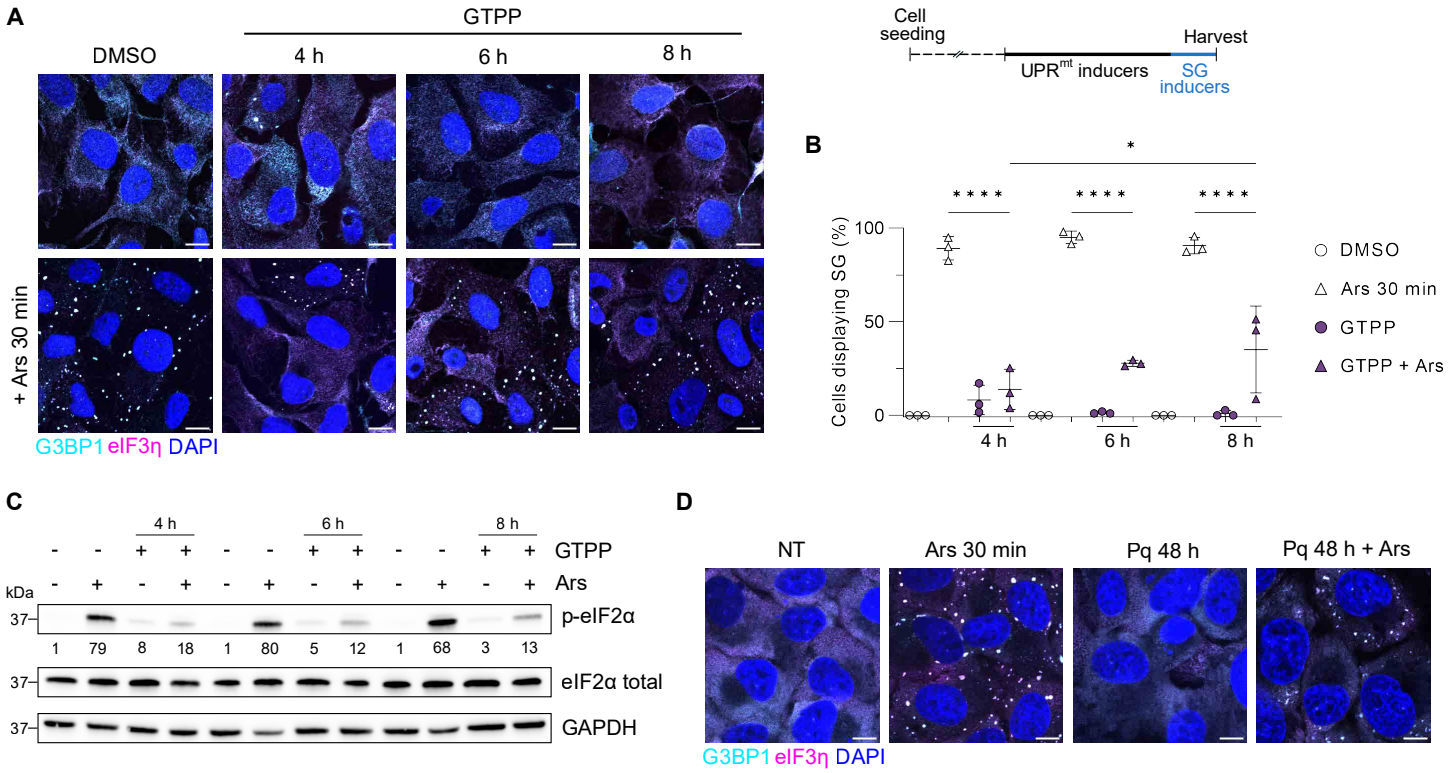
A
GTPP
DMSO
4 h
6 h
8 h
+ Ars 30 min
G3BP1 eIF3η DAPI
Cell seeding
Harvest
UPRmt inducers
SG inducers
B
Cells displaying SG (%)
100
50
0
4 h
6 h
8 h
DMSO
Ars 30 min
GTPP
GTPP + Ars
C
4 h
6 h
8 h
GTPP
Ars
kDa
37
p-eIF2α
1 79 8 18 1 80 5 12 1 68 3 13
eIF2α total
GAPDH
D
NT
Ars 30 min
Pq 48 h
Pq 48 h + Ars
G3BP1 eIF3η DAPI
E
Cells displaying SG (%)
NT
Ars
Pq
Pq + Ars
F
48 h
Pq
Ars
kDa
p-eIF2α
1 79 8 18
eIF2α total
eIF3η
100
G
SG area (μm2)
SG/cell
Ars
Pq+Ars

Figure 4

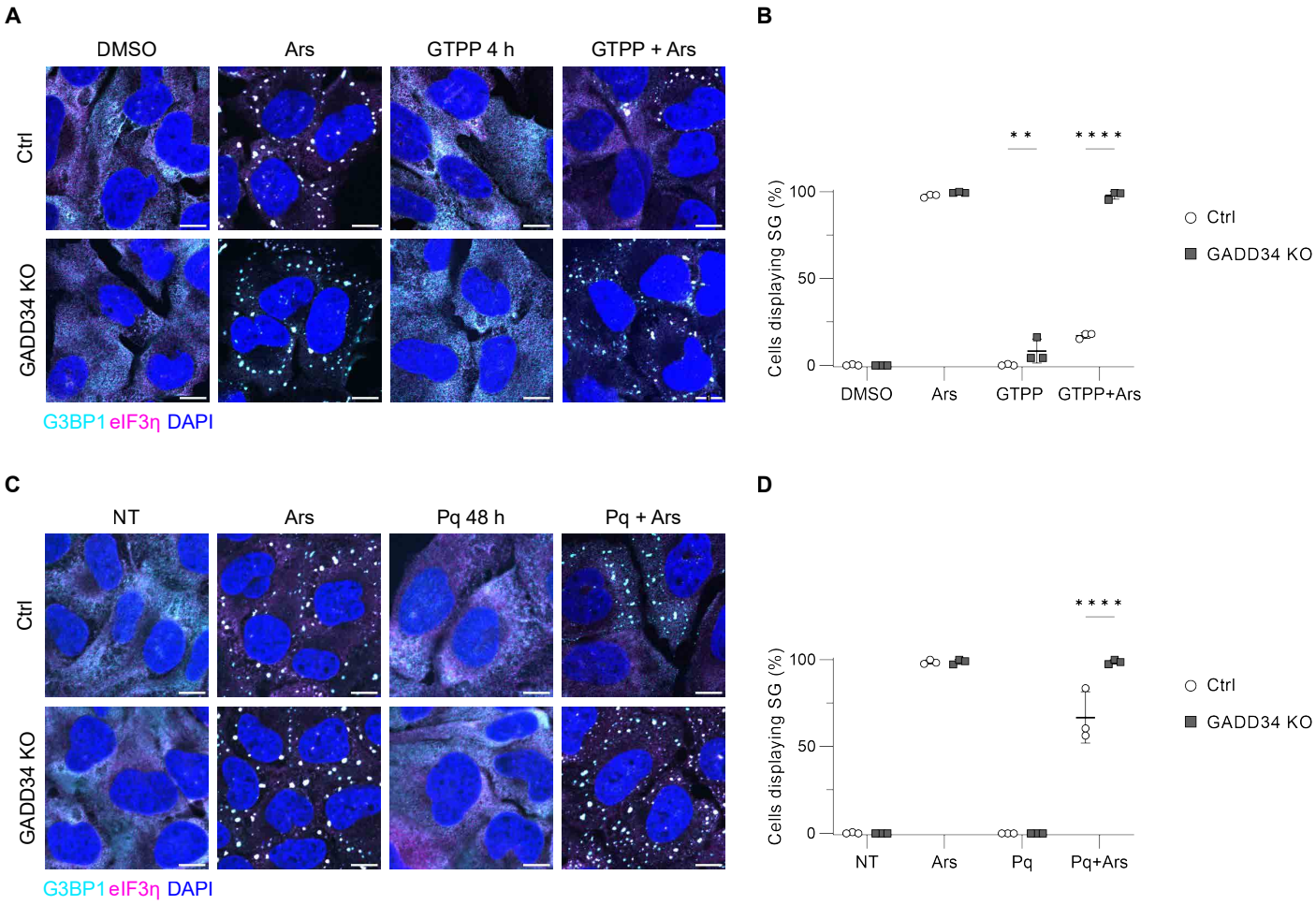
A
DMSO
Ars
GTPP 4 h
GTPP + Ars
Ctrl
GADD34 KO
G3BP1 eIF3η DAPI
B
Cells displaying SG (%)
100
50
0
DMSO
Ars
GTPP
GTPP+Ars
* *
* * * *
Ctrl
GADD34 KO
C
NT
Ars
Pq 48 h
Pq + Ars
Ctrl
GADD34 KO
G3BP1 eIF3η DAPI
D
Cells displaying SG (%)
100
50
0
NT
Ars
Pq
Pq+Ars
* * * *
Ctrl
GADD34 KO

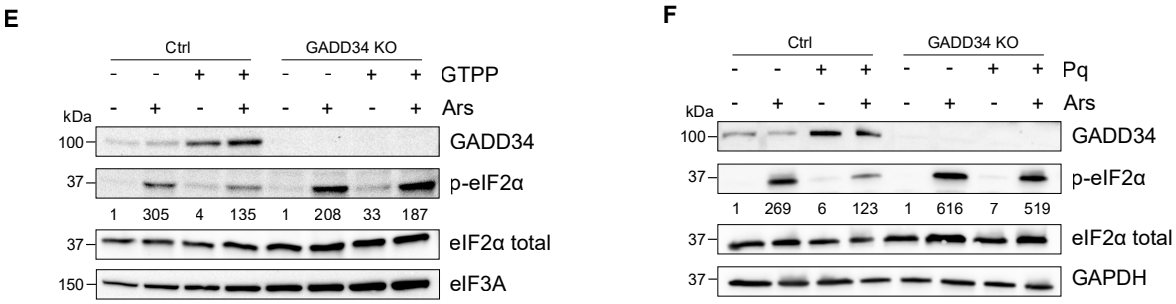
E
Ctrl
GADD34 KO
GTPP
Ars
kDa
100
37
150
GADD34
p-eIF2α
1 305 4 135 1 208 33 187
eIF2α total
eIF3A
F
Ctrl
GADD34 KO
Pq
Ars
kDa
100
37
GADD34
p-eIF2α
1 269 6 123 1 616 7 519
eIF2α total
GAPDH

Figure 5

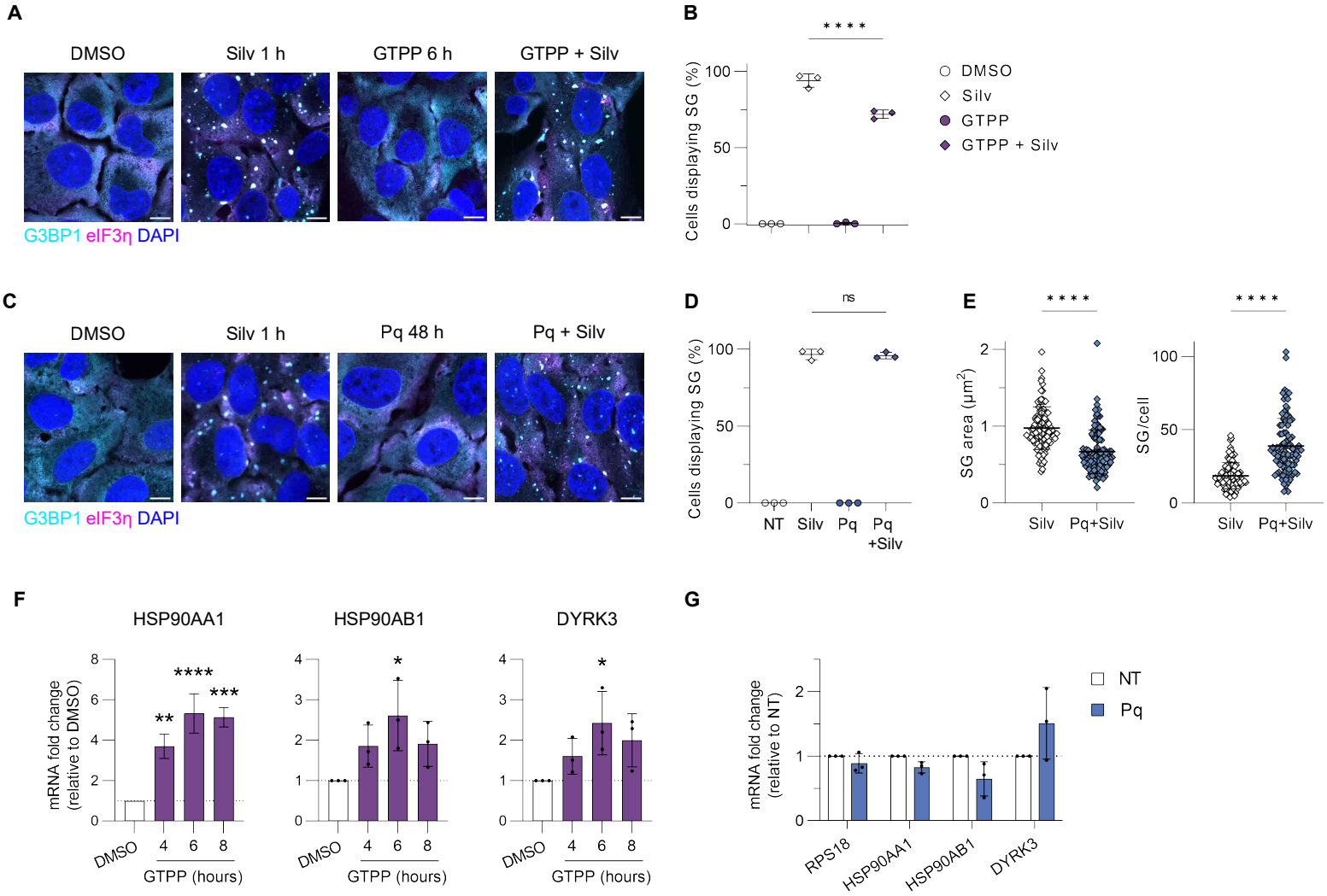
A
DMSO
Silv 1 h
GTPP 6 h
GTPP + Silv
G3BP1 eIF3η DAPI
B
Cells displaying SG (%)
DMSO
Silv
GTPP
GTPP + Silv
C
DMSO
Silv 1 h
Pq 48 h
Pq + Silv
G3BP1 eIF3η DAPI
D
ns
Cells displaying SG (%)
NT
Silv
Pq
Pq +Silv
E
SG area (μm²)
SG/cell
Silv
Pq+Silv
F
HSP90AA1
HSP90AB1
DYRK3
mRNA fold change (relative to DMSO)
DMSO
GTPP (hours)
G
mRNA fold change (relative to NT)
NT
Pq
RPS18
HSP90AA1
HSP90AB1
DYRK3

Figure 6

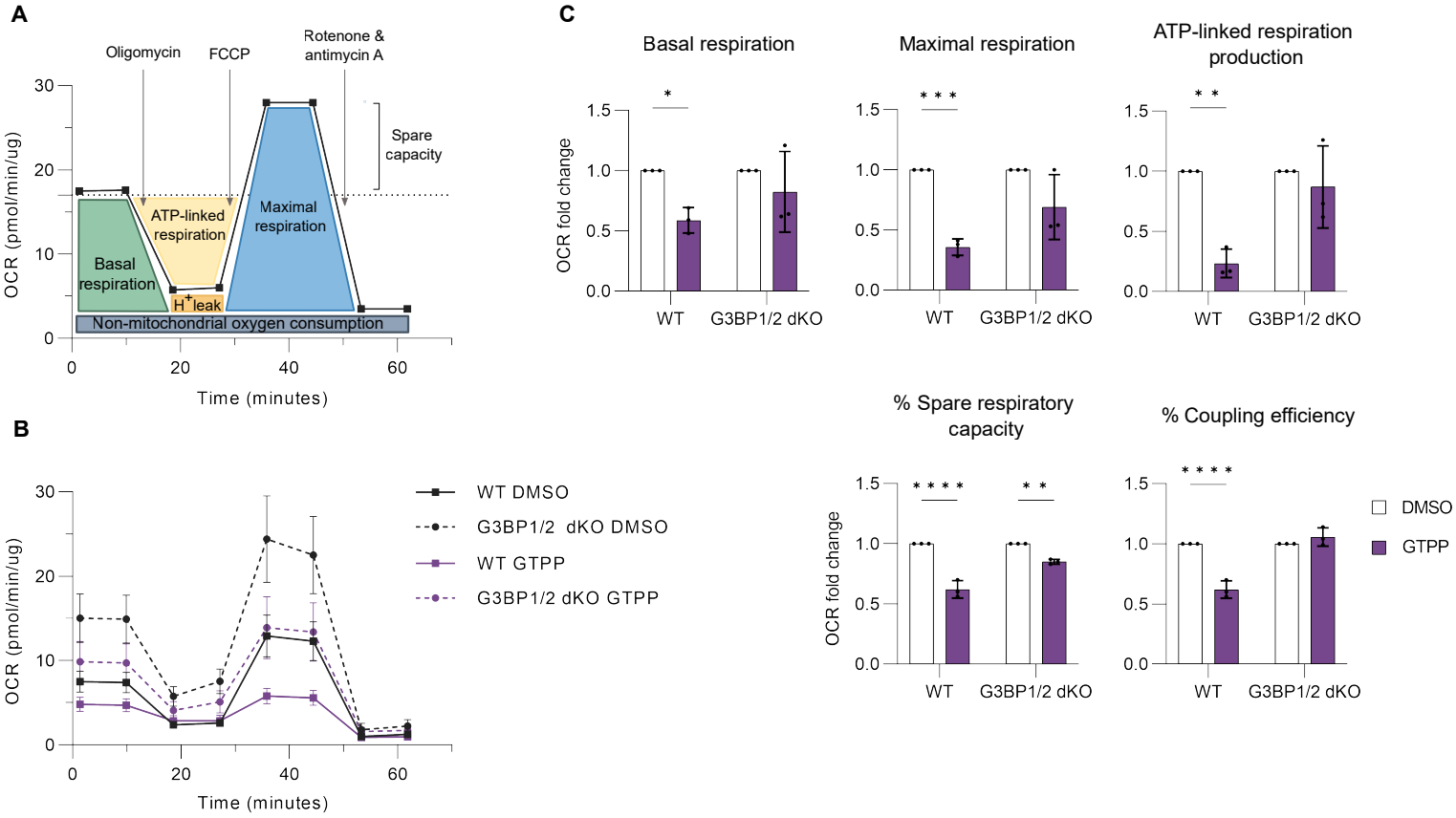
A
Oligomycin
FCCP
Rotenone & antimycin A
Spare capacity
ATP-linked respiration
Maximal respiration
Basal respiration
H+ leak
Non-mitochondrial oxygen consumption
OCR (pmol/min/ug)
Time (minutes)
B
WT DMSO
G3BP1/2 dKO DMSO
WT GTPP
G3BP1/2 dKO GTPP
OCR (pmol/min/ug)
Time (minutes)
C
Basal respiration
Maximal respiration
ATP-linked respiration production
% Spare respiratory capacity
% Coupling efficiency
OCR fold change
WT
G3BP1/2 dKO
DMSO
GTPP